

# Observations of the exchange of ocean waters between the Pacific Ocean and the Gulf of California

Curtis A. Collins<sup>1</sup>, Rubén Castro<sup>2,\*</sup>

<sup>1</sup> Naval Postgraduate School (Rm. 328, 833 Dyer Road - Monterey - CA 93943 - USA)

<sup>2</sup> Universidad Autónoma de Baja California - Facultad de Ciencias Marinas (Carretera Transpeninsular Ensenada - Tijuana No 3917 - Playitas - Ensenada - BC 22860 - México)

\* Corresponding author: [rcastro@uabc.edu.mx](mailto:rcastro@uabc.edu.mx)

## ABSTRACT

Kinematics of seasonal exchanges of mass and heat between the Pacific Ocean and the Gulf of California are described. Results are based on 18 occupations between 1992 and 2013 of a hydrographic section across Pescadero Basin at the mouth of the Gulf and two and a half years (November 2003 to May 2006) of moored velocity and CTD measurements in 130 m of water on either side of the Pescadero Basin. Cyclonic conditions dominated in mid-winter and summer with inflow along Sinaloa and outflow along Baja California Sur (BCS). Advection of warm Gulf waters into the Pacific along BCS in late fall extended the warming along BCS by almost two months compared to Sinaloa; as a consequence, steric heights at BCS were higher, and resulted in near surface transport out of the Gulf of  $\sim 0.01 \text{ m s}^{-1}$ . During warming periods from May through November, coastal trapped waves transported heat into the Gulf along Sinaloa; the trapped wave motions along BCS were about a tenth of the amplitude of those at Sinaloa and contributed little to transport into the Pacific. Poleward monsoon winds were in phase with near-surface geostrophic flows into the Gulf which were about the same magnitude as out flow associated with much stronger equatorward wind. Next to BCS, higher salinity Gulf waters extended to 180 m depth ( $\sim 26.2 \text{ kg m}^{-3}$ ) and flow into the Pacific; these waters can be traced to subduction in the mid-Gulf region and, when they reach the Pacific, flow poleward in the undercurrent. If global warming intensifies the overturning Gulf circulation, lower oxygen and higher salinity waters may be advected northward along the continental shelf of North America.

**Descriptors:** Gulf of California, Seasonal cycle, Exchange of Pacific and Gulf water, Meridional overturning, North American monsoon, Coastal trapped waves, Tropical storm response.

## INTRODUCTION

Pescadero Basin is located at the mouth of the Gulf of California and is about 180 km wide and 3 km deep so waters are easily exchanged with the Pacific Ocean. This exchange is needed to balance both water and heat budgets. Evaporation

removes about one tonne of water per square meter per year from the Gulf which requires an inflow of Pacific water at a rate of  $4.7 \text{ kt s}^{-1}$  ( $1 \text{ kt} = 1 \times 10^6 \text{ kg}$ ). The annual cycle of heat in the Gulf of California requires a mean annual heat loss of  $40 \times 10^{12} \text{ J s}^{-1}$  to the Pacific. The heat loss occurs from mid-July to mid-March and the maximum,  $56 \times 10^{12} \text{ J s}^{-1}$ , is in mid-November (Castro et al., 1994). Heat gain occurs during the rest of the year and is largest in mid-May,  $19 \times 10^{12} \text{ J s}^{-1}$  (ibid).

Submitted: 15-Apr-2022

Approved: 12-Oct-2022

Associate Editor: Ilson Silveira



© 2022 The authors. This is an open access article distributed under the terms of the Creative Commons license.

To better understand these exchanges, a program of measurements was undertaken at the Gulf entrance. Between 1990 and 2013, research vessels sampled a hydrographic section across Pescadero Basin at the mouth of the Gulf of California with high spatial resolution ( $\sim 10$  km, see Fig. 1) a total of 18 times. During 2004 to 2006, moorings were maintained for 30 months in waters 130 m deep near the edge of the continental shelves on either side of Pescadero Basin. Both methods observed temperature, salinity, and either direct current measurements from moorings or geostrophic flow for cruises.

The Gulf consists of a series of basins which increase in depth from 400 m in Wagner Basin at the head of the Gulf to 3000 m for Pescadero Basin (PB) at the mouth (Lavin and Marinone, 2003). The exchange of water from the north to south is constrained by a series of mid-Gulf islands. Mid-Gulf, southern waters are observed to flow northward through straits and over sills near bottom. Strong tidal currents mix bottom waters in the mid-Gulf area, displacing bottom waters

of mid-Gulf basins upward and modifying water properties (increasing salinity, decreasing dissolved oxygen) of Subtropical Subsurface Waters (StSsW) flowing southward (Paden et al., 1991; Simpson et al., 1994; Rosas-Villegas et al., 2018; López et al., 2008, 2021).

Geographical features in Pescadero Basin include Alarcon seamount which rises to within 500 m of the ocean surface and complex continental margins with steep escarpments especially along Sinaloa. The continental shelf is narrow along Baja California Sur (BCS) but wide off Sinaloa (Fig. 1). Winds typically blow along the Gulf, poleward from June through August (the North American monsoon) and equatorward the rest of the year (Bordoni et al., 2004; Marinone et al., 2004). Cyclonic circulation, common at subtropical latitudes along the Eastern Boundary of the Pacific (Munk, 1950), usually occurs year-round in Pescadero Basin (Mascarenhas et al., 2004) with inflow along Sinaloa and outflow along BCS. Strong buoyancy driven exchanges between the Gulf and Pacific Ocean occur in Pescadero Basin

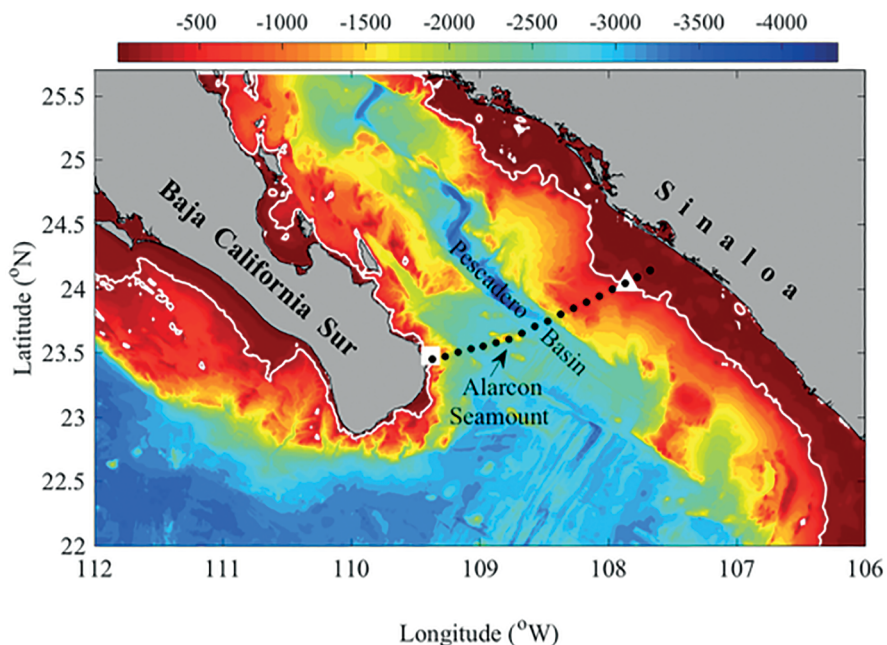


**Figure 1.** Chart showing the bathymetry and measurement locations in Pescadero Basin (PB) at the entrance to the Gulf of California. Black dots are locations of hydrographic measurements and white square (triangle) show the location of moorings at Cabo Pulmo (El Dorado). The color bar at the top indicates water depth and the continental shelf is delimited by a white line, the 200 m isobath.

in May (November) when Pacific waters warm (cool) the lower Gulf (Castro et al., 1994; Beron-Vera and Ripa, 2000). Coastal trapped waves, generated by tropical storms off southern Mexico and in the Eastern Tropical Pacific, are observed to propagate into the Gulf along the Sinaloa shelf (Christensen et al., 1983; Merrifield and Winant, 1989; Martinez and Allen, 2004; Zamudio et al., 2008; Gutiérrez et al., 2014). Strong cyclonic flow has been observed at the Gulf entrance (Roden, 1972; Collins et al., 1997; Mascarenhas et al. 2004; Zamudio et al., 2008; Collins et al., 2015).

Two saline water masses are formed within the Gulf, warm summer surface waters referred to as Gulf of California Water (GCW) and a Subtropical Subsurface Water (SSW) which is formed in the mid-Gulf region (referred to as Central Gulf Water by Bray, 1988). These are exchanged with a variety of Pacific waters: Tropical Surface Water (TSW), Subtropical Subsurface Water (StSsW), and California Current water (CCW) (Stevenson, 1970; Torres-Orozco, 1993; Castro et al., 2000, 2017; Lavín et al., 2009; Collins et al. 2015; Portela et al., 2016). Here observations are used to describe these exchanges of mass and heat.

## METHODS

The goal of our measurements was to observe the spatial and temporal structure of the exchange of water between the Gulf of California and the Pacific Ocean. Accordingly, observations were made at the mouth of the Gulf of California (Figure 1). The first measurements were hydrographic sections across Pescadero Basin (PB) in 1992 (Collins et al., 1997); this section was resampled a total of 18 times, ending in 2013 (Castro et al., 2017; Larios-Muñiz et al., 2022). During a 2.5-year period from 2003 to 2006, single moorings were deployed on the continental shelf on either side of the Pescadero Basin section (Figure 1). Water properties in this study use TEOS-10 (IOC et al., 2010) and include Conservative Temperature ( $\Theta$ , °C), Absolute Salinity ( $S_A$ , g kg<sup>-1</sup>), Preformed Salinity ( $S$ ), pressure ( $p$ , dbar) and *in situ* density  $\rho(S_A, \Theta, p)$  and density anomaly ( $\sigma(S_A, \Theta, p)$ , kg m<sup>-3</sup>). Additional details are given below.

## PESCADERO BASIN SECTION

A mean flux of mass and heat for a hydrographic section that spans the entrance to the Gulf is estimated below. The location of the section is shown in Figure 1 and consisted of 20 hydrographic stations spaced about 10 km apart. At these stations, CTD casts measured continuous vertical profiles of temperature, salinity, and pressure. The section was occupied eighteen times and are listed chronologically in Table 1. Maximum sampling depth is also noted Table 1. Data for U.S. research vessels is available from both U.S. and Mexican data centers and observations by Mexican vessels are available from the Mexican data center.

The hydrographic data for individual cruises were objectively mapped (see Castro et al., 2000) onto an 80 (5 dbar pressures) x 18 grid that spanned PB and extended from the surface to 400 dbar. The first section was in May 1992 and the last in April 2013. Upper ocean temperature and density were dominated by an annual cycle which varied from year to year and these cruises did not resolve year to year variations of the annual cycle. To construct the annual mean field, a biharmonic (annual and semiannual cycles) least squares fit was made to the time series of  $\Theta$  and  $S$  at each grid point (Chelton, 1984). The mean field was smoothed horizontally with a fourth order low pass Butterworth filter with a cut off at 67 km, about twice the 35 km Rossby internal radius of deformation (Chelton et al., 1998). Note that  $S$  was used for individual cruises but the mean  $S$  was converted to  $S_A$  for the figures below (IOC, SCOR and IAPSO, 2010).

## MOORED TIME SERIES

Intermediate moorings were deployed on both sides of the Gulf in water 130 m deep. The moorings were 105 m long and included upward looking acoustic Doppler current profilers (ADCP) a few meters above the anchor as well as three microcats (measuring temperature, conductivity and pressure) at nominal depths of 40, 80, and 120 m. The sampling rate for the ADCP was every 15 minutes while the microcats sampled every 5 minutes (microcat data and processed ADCP data are available from the authors). One mooring was

**Table 1.** List of the cruises across Pescadero basin. The cruises are ordered by month and day.

Month	Day	Year	Cruise	Depth (m)	Ship
Feb	8-9	1994	P04	bottom	F. de Ulloa
Feb	28-29	2013	P13	bottom	F. de Ulloa
Mar	14-15	2002	P14	700	Río Suchiate
Apr	14-15	2013	P24	bottom	Point Sur
May	2-4	1992	P01	bottom	DeSteiger
May	18-19	2004	P17	1700	F. de Ulloa
May	28-30	1998	P11	bottom	F. de Ulloa
Jun	7-8	2004	NAME1	1500	F. de Ulloa
Aug	2-4	1998	P12	bottom	F. de Ulloa
Aug	10-11	2004	NAME2	1000	F. de Ulloa
Aug	13-15	1995	P07	bottom	El Puma
Oct	15-16	2002	P15	700	Río Suchiate
Oct/Nov	31-1	1994	P05	1200	A. Humboldt
Nov	5-6	2003	P16	1500	Point Sur
Nov	16-17	2004	P18	bottom	Point Sur
Nov	19-20	1997	P10	bottom	F. de Ulloa
Nov	26-27	2005	P20	1000	F. de Ulloa
Dec/Jan	29-1	1992	P02	bottom	Point Sur

located off Cabo Pulmo (CP), Baja California Sur, at 23° 28.66'N, 109° 22.94'W, in a marine conservation area where fishing was not permitted. The second mooring was located on the Sinaloa shelf to the west of El Dorado (ED) at 24° 02.150'N, 107° 51.402'W (see Fig. 1). While the water depth was similar, the bathymetry was not: the shelf off BC was quite narrow while that off Sinaloa was broad, possibly isolating nearshore flows from those over the outer shelf and slope.

The moorings were first deployed on 4 November 2003 and after five successive six-month deployments, were retrieved on 6 May 2006. Data were collected successfully for each ED deployment. But the ADCP at CP failed for the first setting and no microcats were available for the fourth setting (mid-May through November 2005); the only observed temperatures during the fourth setting were collected by the ADCP at a depth of  $126.1 \pm 0.3$  m. The upward-looking ADCPs collected velocity profiles slightly longer than 100 m with 4 m resolution. Instruments were calibrated and serviced before deployment and checked using *in-situ* shipboard CTD casts before or after mooring retrieval.

The moored data were assembled into a continuous time series. A principal component analysis was used to identify the alongshore component of flow: a mathematical rotation of  $-65.3^\circ$  ( $-21.2^\circ$ ) for CP (ED). The alongshore velocity observations were chosen to span depths from 20 to 120 m. For flux estimates, microcat data were linearly interpolated to the same depths, 20 to 120 m. Gaps between moorings were filled by interpolation for temperature, salinity and velocity. Valverde-Kalish (2016) also analyzed the mooring data and include additional details and statistics including empirical orthogonal function analysis.

To fill the gap in microcat data for mid-May to mid-November 2005, models for daily temperature and geopotential at 40 and 80 m were constructed using observations for the same period in 2004. Multivariable,  $y = a_0 + a_1x_1 + a_2x_2$ , and single variable,  $y = a_0 + a_1x_1$ , models were derived using a least squares fit; for the 80 m model, variables were  $y = 80$  m temperature/geopotential,  $x_1 = 120$  m temperature/geopotential, and  $x_2 = \text{time (days)}$ . Both models yielded similar results; the RSME was  $0.25^\circ\text{C}$  for both 40 and 80 m, so the single variable model was used. Salinity was not correlated

with 120 m temperatures, so the mean salinity for the summer/fall 2004 was used to estimate geopotential for the same period in 2005.

Satellite measurements of geostrophic surface circulation in PB were derived from daily Absolute Dynamic Topography (ADT) estimates for a  $0.25^\circ \times 0.25^\circ$  spatial resolution (Copernicus Marine Services, <http://marine.copernicus.eu>) and are based upon along track data that have a repeat period of nearly ten days (Valle-Rodríguez and Transviña-Castro, 2017). Hourly atmospheric sea level pressure data were obtained from ERA5 reanalysis (<https://cds.climate.copernicus.eu/>; accessed 15 January 2021) for a  $0.25^\circ \times 0.25^\circ$  grid, while wind data were obtained from the reanalysis Cross-Calibrated Multi-Platform Wind Vector Analysis Product (CCMP) which provided wind vectors at 10 m above the sea surface every six hours for a  $0.25^\circ \times 0.25^\circ$  grid (Atlas et al., 2011). The wind stress was computed following Trenberth et al. (1990).

## RESULTS

### PESCADERO BASIN SECTIONS

The relationship between observations of  $\Theta$  and  $S_A$  collected by hydrographic casts are shown in Figure 2 and illustrate the variability of water mass properties observed in Pescadero Basin. Waters less dense than  $23 \text{ kg m}^{-3}$  were a mixture of Tropical Surface (TSW) and Gulf of California Waters (GCW). Between  $24 \text{ kg m}^{-3}$  and  $25 \text{ kg m}^{-3}$ , waters included some California Current water (CCW), more GCW and largely a mixture of the two waters between  $34.6$  and  $35.1 \text{ g kg}^{-1}$ . Between  $25 \text{ kg m}^{-3}$  and  $26.7 \text{ kg m}^{-3}$ , Subtropical Subsurface Waters (StSsW) were dominant although a small number of CCW observations and some GCW were observed between these density surfaces; note that mixing of CCW and GCW would create waters with T/S similar to StSsW (Castro et al., 2000).

Deeper waters, Pacific Intermediate (PIW) and Deep Water (PDW), were not included in this study in part because Gulf of California processes have little effect on these deeper waters but also because these waters were not sampled on all cruises (Table 1). Roden (1972) observed

that deeper waters were warmer in this region (waters were cooler below 2500 m to the west of  $18^\circ\text{N}$ ,  $111^\circ\text{W}$ , about 500 km from PB). A number of active geothermal vents have been recently observed in Pescadero Basin (Paduan et al., 2018) which could contribute to the warming of deeper waters in PB.

Mean water properties are shown for sections across Pescadero Basin in Figure 3. Isotherms (Fig 3a) and isopycnals (Fig 3c) were similar at a given depth. For the upper 50 dbar, isotherms and isopycnals sloped upward at each coast but at greater depths, they sloped downward at each coast. The former pattern is anticyclonic, caused by coastal upwelling or coastal flow directed out of (into) the Gulf off Sinaloa (Baja California Sur). The deeper pattern corresponds to cyclonic flow.

Salinity identifies the source of the water and generally the direction of its along Gulf motion. Higher (lower) salinity waters form in the Gulf (Pacific Ocean) and subsequently flow through Pescadero Basin into the Pacific Ocean (Gulf). Salinity mean field has a small range across Pescadero Basin (Fig. 3b) which is maximum,  $0.2 \text{ g kg}^{-1}$ , between  $15^\circ\text{C}$  and  $19^\circ\text{C}$  so horizontal pressure differences are mostly due to temperature changes. The salinity distribution shows four well defined layers. On the western or Baja California Sur (BCS) side of the section, salinity maxima are seen at the surface and about 150 dbar, representing more saline Gulf of California waters. These two salinity maxima are separated at 50 dbar where an intrusion of fresher waters extended westward from the Sinaloa coast. These fresher waters are characteristic of the Pacific, either Subarctic waters carried southward by the California Current (Castro et al., 2017; Larios-Muñiz et al., 2022) or Tropical Pacific waters carried northward by the Mexican Coastal Current (Lavín et al. 2006; Portela et al., 2016). The deepest layer begins about 250 dbar where the salinity ( $<34.85 \text{ g kg}^{-1}$ ) is nearly uniform across the section and decreases as pressure increases to the core of Pacific Intermediate Water at about 500-600 m (Spearman, 1993; Portela et al., 2016). The salinity distribution (Fig. 3b) suggested that higher salinity Gulf and Subtropical Subsurface Water extended from the surface to a pressure of  $<200$  dbar along the Baja coast.

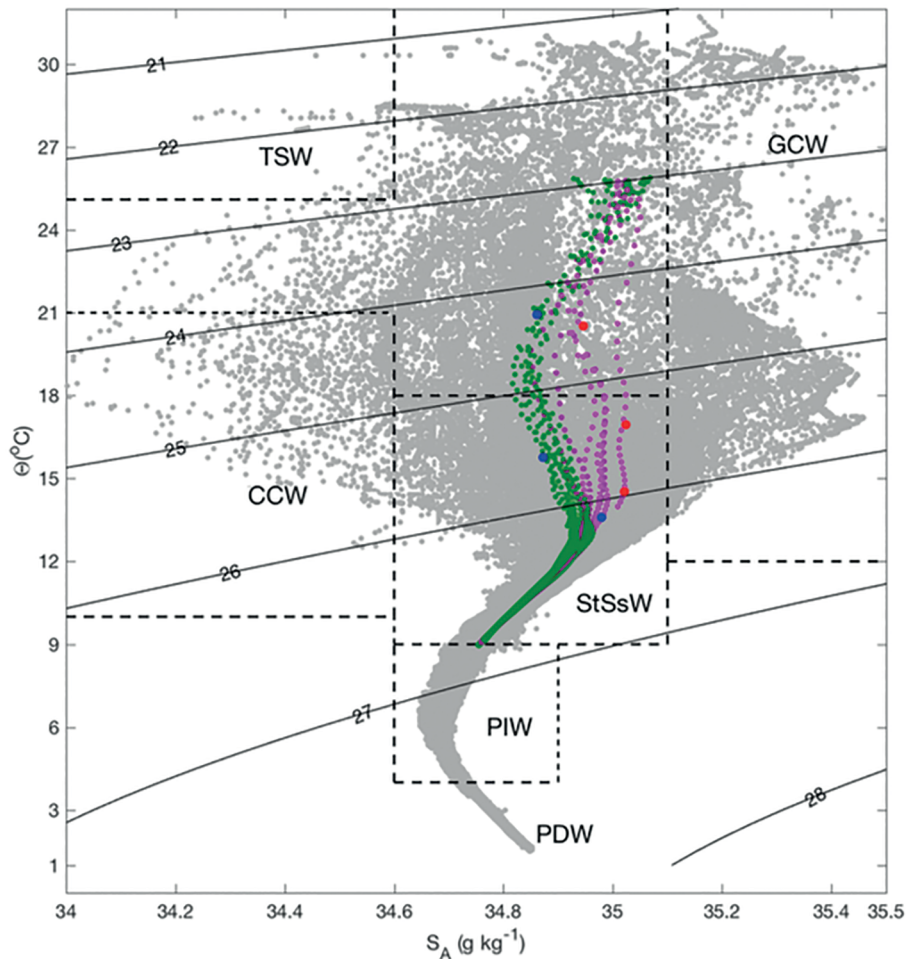


**Figure 2.** Conservative Temperature and Absolute Salinity diagram. Grey dots are observations collected at 2 dbar intervals from the surface to the bottom for CTD casts from 18 cruises listed in Table 1. Green and magenta dots are the annual mean of data which have been objectively mapped for the cross-Gulf section (Fig. 1) with a 5 m vertical resolution to a maximum depth of 400 m. Green dots represent geostrophic inflow water and red dots are waters which are flowing out of the Gulf. The closed blue (red) circles are annual means for moored measurements at 40, 80, and 120 m for ED (CP). Black lines represent density anomalies ( $\text{kg m}^{-3}$ ). Water mass characteristics are enclosed by dashed lines (Portela et al. 2016): Tropical Surface water (TSW), Gulf of California water (GCW), California Current Water (CCW), Subtropical Subsurface Water (SSW), Pacific Intermediate (PIW) and Pacific Deep Water (PDW).

Geostrophic currents are shown along isobaric surfaces in fig. 3d. The zero isotach at  $108.72^\circ\text{W}$  was nearly vertical and lies above the summit of Alcaron seamount (see Fig. 1), separating inflow to the east of the seamount from the outflow to the west (Mascarenhas et al., 2004). A similar zero isotach was observed on three cruises where direct measurements of velocity were made for the entire water column (April 1992, May 1992, January 1993, Collins et al., 1997). At BCS, geostrophic outflow (Fig. 3d) was found at the coast below 10

m and was greatest at 80 m,  $>7 \text{ cm s}^{-1}$ . The maximum velocity off Sinaloa,  $>5 \text{ cm s}^{-1}$ , occurred in a 10 km wide band, which extended from the sea surface at  $108.4^\circ\text{W}$  downward and eastward, intersecting the Sinaloa shelf between 50 dbar and 140 dbar. Also note a wedge of weak inflow next to the upper Sinaloa margin below 320 dbar; this is located near an unnamed subsurface ridge which extends upward from the seafloor to 450 m depth. Similar outflows along the upper continental margin of Sinaloa were observed on April 1992, May

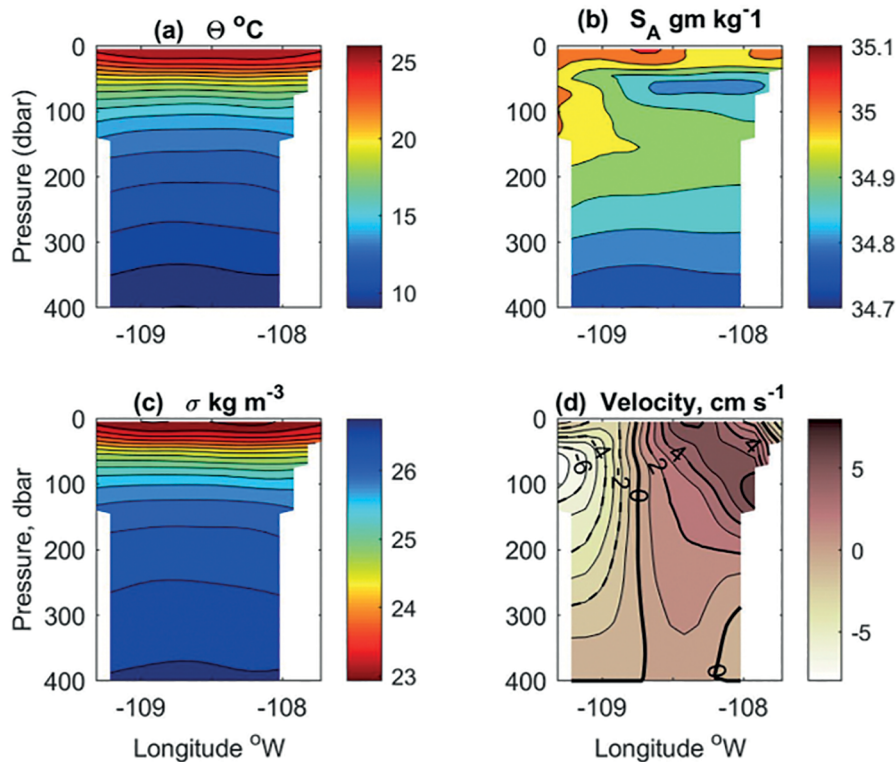


**Figure 3.** Isobaric views of mean water properties for the Pescadero Basin transection. (a) Conservative Temperature, contour interval is 1°C. (b) Absolute Salinity, contour interval is 0.05 g kg<sup>-1</sup>. (c) *In situ* density, contour interval is 0.25 kg m<sup>-3</sup>. (d) Geostrophic velocity referenced to 400 dbar. The contour interval is 1 cm s<sup>-1</sup>.

1992, and January 1993 cruises (Collins et al., 1997; Mascarenhas et al., 2004). Finally, at the sea surface next to Sinaloa, a 10-dbar thick lens of 34 g kg<sup>-1</sup> salinity occurred, imbedded in a weak outflow over the inner shelf.

Geostrophic velocities (Fig. 3d) were used to calculate heat and mass fluxes across the PB section following Bacon and Fofonoff (1996). A mass transport of 4.7 kt s<sup>-1</sup> (1 kt = 10<sup>6</sup> kg) is needed to balance the mean rate of evaporation (E) minus the sum of precipitation (P) and river outflow (R) for the Gulf. The vertical profile for mass transport using the geostrophic velocity field (Fig. 3d) indicated inflow above 257.5 m and outflow below (the red profile in Fig. 4a). When summed vertically, it yielded a mass transport of 179.6 kt s<sup>-1</sup>, much greater than the 4.5 kt s<sup>-1</sup> required to balance the freshwater budget of the Gulf. Geostrophic velocities can be adjusted using a level of known motion or adding barotropic flow. Using the velocity data at the sea surface observed by satellite altimeter

as a level of known motion yielded an unrealistic net mass transport of -189 kt s<sup>-1</sup>. This was unexpected given the good agreement for sea level slope for satellite and moored measurements reported below.

Barotropic corrections to the geostrophic velocities were necessary to achieve a net mass flux of 4.5 kt s<sup>-1</sup>. Several were suggested by previous observations of deeper PB sections (Sverdrup, 1939; Roden, 1959; Warsh and Warsh, 1971) and velocity observations (Collins et al., 1997). These included 1) maximum outflow near the western boundary at the Baja coast, 2) maintaining the position of the transition between outflow and inflow near 108.7°W, and 3) keeping the inflow to the east of 108.7°W at 400 dbar ≥ 0. The simplest correction, an addition of a constant velocity of -0.28 cm s<sup>-1</sup> at the level of no motion (400 dbar) across the entire section, balanced the mass transport but resulted in outflows at depth to the east 108.7°W.

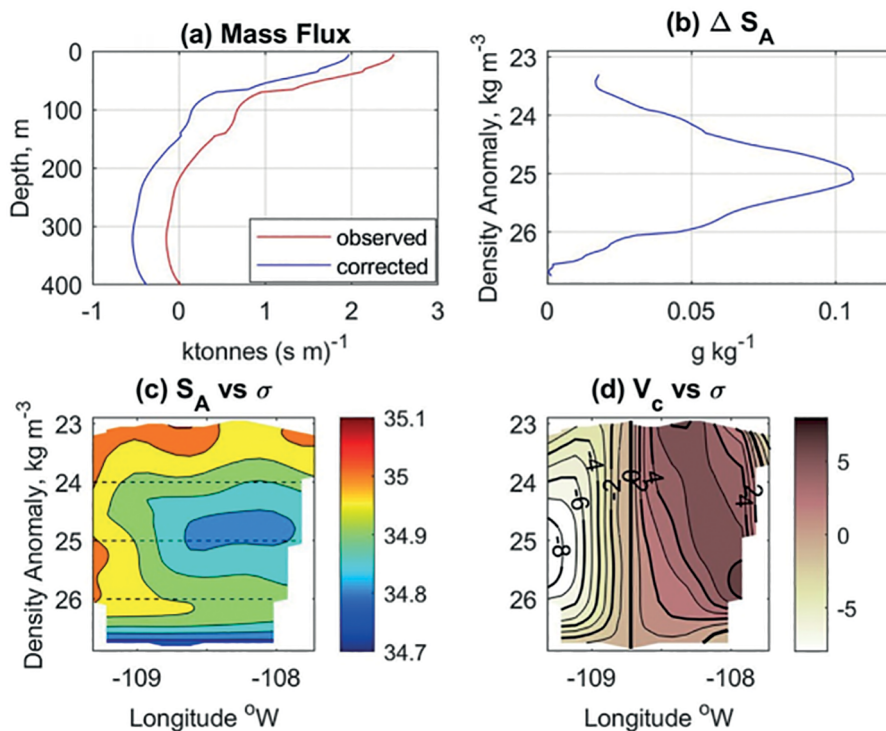


**Figure 4.** Pescadero Basin section properties. (a) Geostrophic observed (red line) and corrected profiles (blue line) for mass transport; the corrected profiles have a net mass transport of 4.5 kt s<sup>-1</sup> for the upper 400 dbar. (b) Differences of salinity (outflow minus inflow) along isopycnals. Data were calculated every 0.05 kg m<sup>-3</sup>. (c) Mean salinity distribution on isopycnals. The color bar shows salinity values and the contour interval is 0.05 g kg<sup>-1</sup>. (d) Corrected geostrophic velocity for waters shallower than 400 dbar across the Pescadero Basin section. The thicker black line is the zero isotach. Velocity contours are 1 cm s<sup>-1</sup>.

As noted above, the outflow was greatest on the Baja shelf and upper slope (Fig 3d), so adding the greatest negative correction there and tapering it to zero at the inflection between the negative and positive flow would preserve the location of the mid-Gulf zero isotach as well as increase the outflow on the BCS shelf to a velocity similar to that shown for CP in Figure S5a. Using Gaussian weights 1, 0.8226, 0.4578, 0.1724, and 0.0439 for geostrophic estimates for stations 2 to 6, respectively, required a corresponding barotropic velocity correction of -1.14, -0.96, -0.59, -0.31, -0.18 cm s<sup>-1</sup>. The corrected vertical profile for this mass transport is shown as the blue line in Figure 4a; the inflow has shoaled to 150 m and 7 kt s<sup>-1</sup> are required to balance inflow and outflow. Other weights (e.g., triangular, Hann, Blackman, Hamming) were applied as barotropic velocity corrections to the outflow and yielded similar results. Net heat flux was  $5.3 \times 10^{12}$  J s<sup>-1</sup>.

Salinity and corrected geostrophic velocities for the Pescadero Basin section are shown on isopycnals in Figures 4c-d. These figures show the symmetry of both the velocity field (inflow to the east, outflow to the west) and salinity (lower salinity to the east, higher salinity to the west). Water properties for inflow (green) and outflow (red) are also shown in Figure 2; waters with density greater than 26.2 kg m<sup>-3</sup> had similar temperature and salinity but outflowing waters with densities between 23 and 26.4 kg m<sup>-3</sup> had greater salinity than inflow (fig 2). In Figure 4c the halocline appears as distinct layers and, except at the western boundary, features were aligned along isopycnals. Near surface, high salinity (35 g kg<sup>-1</sup>) waters spread from west to east at densities 23.1 to 23.4 kg m<sup>-3</sup> but extended deeper to 24.0 kg m<sup>-3</sup> at the Baja coast. Below the upper layer, lower salinity waters, 34.8 g kg<sup>-1</sup>, with density 24.8 kg m<sup>-3</sup> extended westward from Sinaloa to 108.7°W but the salinity minimum

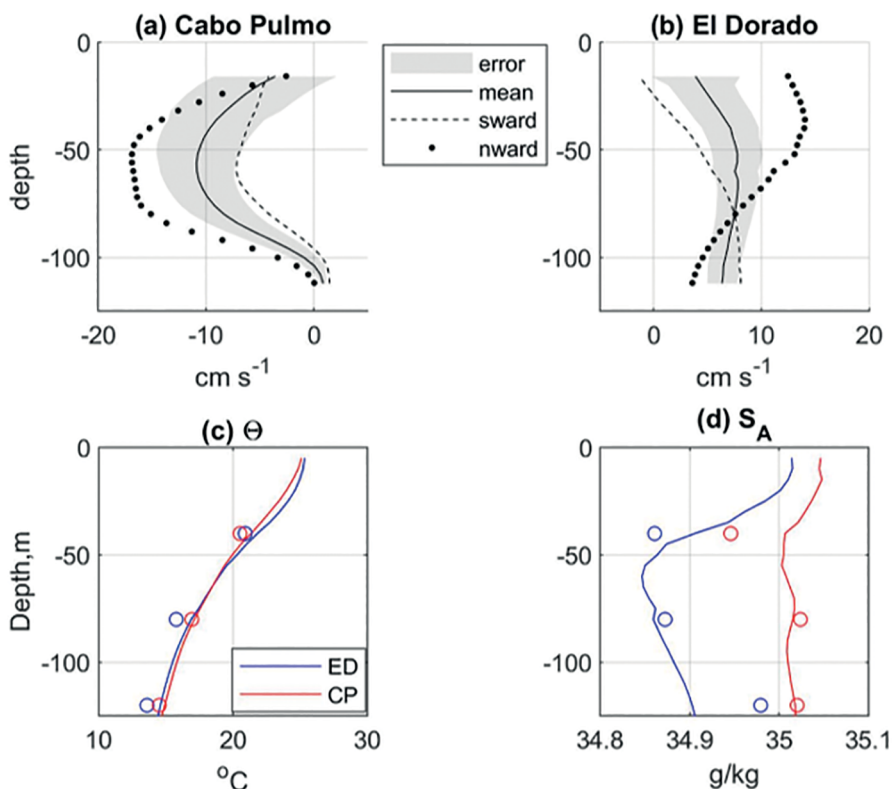


**Figure 5.** Mean conditions at mooring locations. Mean velocity profiles for the period 18 May 2004 to 5 May 2006 are shown for (a) Cabo Pulmo and (b) El Dorado. The mean velocity is shown by the black line and the standard error of the mean is indicated by the shaded area. Conditional samples for periods of seasonal equatorward (sward) and poleward (nward) wind stress are indicated by dashed and dotted lines, respectively. (c) Yearly mean Conservative Temperature and (d) Absolute Salinity at Cabo Pulmo (red) and El Dorado (blue); moored measurements are indicated by circles and the solid lines represent mean values for shipboard CTD casts at mooring locations.

continued to the BCS coast, separating the upper and deeper layers. The third layer was centered on the 26.0 kg m<sup>-3</sup> isopycnal with salinities of 34.95–34.9 g kg<sup>-1</sup> decreasing toward Sinaloa.

Salinity was averaged separately for inflow and outflow along isopycnals and the difference, outflow minus inflow, is shown in Figure 4b and was positive for isopycnals that spanned the PB section. The maximum difference, 0.12 g kg<sup>-1</sup>, was associated with lower salinity waters along the 25 kg m<sup>-3</sup> isopycnal. These values are consistent with salinity differences reported by Roden and Groves (1959) and Collins et al. (1997). Note that the higher salinity along isopycnals meant that temperature was greater in the outflow. The profile for temperature difference (not shown) is similar to that shown for salinity in Figure 4b with the largest

temperature change,  $\Delta\Theta = 0.36^{\circ}\text{C}$  on the 25 kg m<sup>-3</sup> isopycnal.

### MOORED TIME SERIES

Discussion of moored time series focuses on lower frequency events. Mean and seasonal conditions are described as are intraseasonal coastal trapped waves and the variability of the surface and 20 m geostrophic flow between the moorings. Tides and inertial period currents were well resolved by moored measurements but had little effect on net flux at weekly time scales.

### MEAN CONDITIONS

Mean profiles of inflow for a common observation period (18 May 2004 to 5 May 2006, 13 days short of 2 years) are shown in Figure 5. The

means of the two velocity profiles,  $-6.74 \text{ cm s}^{-1}$  at Cabo Pulmo (CP) (fig. 5a) and  $6.80 \text{ cm s}^{-1}$  at El Dorado (ED) (fig. 5b), were indicative of mean cyclonic flow at the Gulf entrance, a pattern discussed in Mascarenhas et al. (2004). The absolute value of the averages was statistically indistinguishable from one another, indicating small net transport between the two shelves. But the transports were only balanced at 18 and 83 m, between these depths CP outflow exceeded ED inflow and at other depths, ED inflow was greater. The CP profile (fig. 5a) indicated a subsurface jet with a minimum speed of  $-10.9 \text{ cm s}^{-1}$  at 56 m and a weak reversal of flow below 100 m. The mean velocities at ED (fig. 5b) encompassed a smaller range than those at CP, from a minimum of  $3.9 \text{ cm s}^{-1}$  at 16 m to  $7.8 \text{ cm s}^{-1}$  at 64 m.

Estimates of the standard error of the mean currents are also shown in Figures 5a-5b. The number of independent samples at each depth was determined by dividing the length of the time series by the lag of the first zero crossing of the velocity autocorrelation. It was clear that above 86 m, velocity perturbations were greater at CP (Figure 5a) than ED (Figure 5b) but near the bottom CP variability was less than ED.

Mean profiles for Conservative Temperature and Absolute Salinity are shown in Figures 5c-5d. Here moored values are compared with average vertical profiles derived for stations 1 and 16 along the Pescadero Basin section Figures 3a-3b. Both data sets show the mean temperature of water above (below) about 60 m to be slightly warmer (cooler) at ED than CP (Figure 5c). The variability of the mean salinity values (Figure 5d) was quite small, ranging from  $34.86 \text{ g kg}^{-1}$  to  $35.02 \text{ g kg}^{-1}$ . For ED (CP) the difference in mean CTD and moored temperature measurements was about  $1^\circ\text{C}$  ( $0.5^\circ\text{C}$ ) and for salinity was  $0 \text{ g kg}^{-1}$  ( $-0.15 \text{ g kg}^{-1}$ ) at 80 m and 120 m and  $0.06 \text{ g kg}^{-1}$  ( $0.05 \text{ g kg}^{-1}$ ) at 60 m. The vertical temperature gradients at ED (CP) were similar,  $0.085 \text{ }^\circ\text{C m}^{-1}$  ( $0.077 \text{ }^\circ\text{C m}^{-1}$ ).

## SEASONAL VARIABILITY

The variability of the moored time series is shown in Figure 6 for vertically averaged Conservative Temperature, Absolute Salinity and inflow as well as perturbations of bottom pressure for El Dorado

and Cabo Pulmo. The time series of averaged data have been smoothed so as to remove fluctuations with frequencies greater than one cycle per three weeks. The biharmonic (annual + semiannual) least squares fit to the temperature, salinity and inflow time series are also shown. The vertical solid (dashed) lines in Figure 6 indicate mid-November and mid-May when the maximum exchanges of heat between the Pacific Ocean and Gulf are expected to occur (Castro et al., 1994).

The temperature time series (Figure 6a) had a well-defined annual cycle: the biharmonic fit accounted for 73% (64%) of the variance at CP (ED). The seasons were extended at CP as Gulf waters flow into the Pacific. As a result, the ED temperatures lead those at CP by 51 days. During warming periods from May to October, ED was slightly warmer than CP. Temperature differences between CP and ED were greatest in November/December when temperatures cooled at ED; subsequently there was a period of one to six months before temperatures at ED were similar to those at CP. The warmest CP (ED) temperature,  $21.64^\circ\text{C}$  ( $20.18 \text{ }^\circ\text{C}$ ) was observed on 24 November 2003 (24 October 2004). During the common 2-year measurement period, the CP mean temperature was  $17.16^\circ\text{C}$  compared to  $16.53^\circ\text{C}$  at ED.

The initiation of fall cooling at ED was due to advection of Pacific waters into the Gulf. The length of this cooling varied from year to year and the best example of late fall cooling at ED occurred in October and November 2005. At ED, the temperatures shown in Figure 6a decreased from  $18^\circ\text{C}$  to  $13.69^\circ\text{C}$  (the coldest ED temperature in the time series) in a month; the temperatures at CP followed this temperature drop, reaching  $15.3^\circ\text{C}$  on 12 November and subsequently warmed to  $20.14^\circ\text{C}$  on 6 December while the temperature at ED warmed to  $14.73^\circ\text{C}$ . The cooling in 2003 and 2004 took place in smaller steps but was preceded by two small warming fluctuations of less than  $1^\circ\text{C}$  a month apart followed by a temperature decrease of  $4\text{-}5^\circ\text{C}$ .

In the middle of winter (January/February), the temperatures at ED also behaved in a non-seasonal manner, increasing  $\sim 2^\circ\text{C}$ , matching temperatures at CP, and subsequently cooling at the same rate as CP until both time series reach minimum

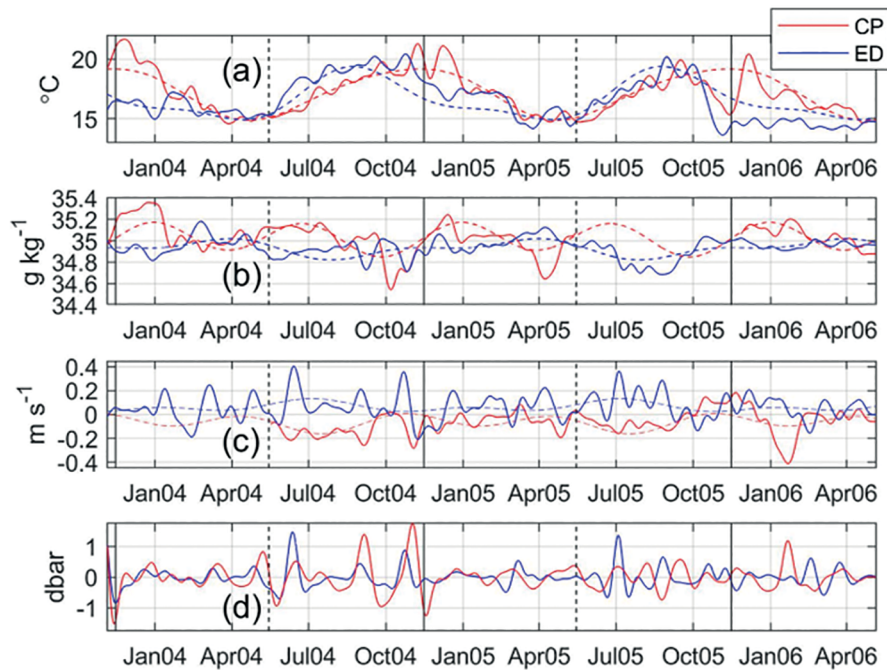


**Figure 6.** Moored time series of vertically averaged Conservative Temperature (a), Absolute Salinity (b), inflow (c) and pressure anomalies (d) for Cabo Pulmo (CP, red) and El Dorado (ED, blue). The pressure anomalies at CP were multiplied by ten so that they could easily be compared to other time series. Dashed lines in the upper three panels are biharmonic fits of the annual and semiannual frequencies. Vertical black solid (dashed) lines mark 15 November (15 May) when cold (warm) Pacific waters usually enter the Gulf.

yearly values in March. Like the early fall cooling, the mid-winter temperature increase at ED should also be the consequence of a change in the character of inflowing

A seasonal cycle for the vertically averaged absolute salinity time series (Figure 6b) was less pronounced, accounting for only 43% of the variability of the time series at both mooring sites. At CP the biharmonic fit had a semiannual fluctuation with greatest (lowest) salinity in January and July (April and October). The range of CP salinities hovered near  $35 \text{ g kg}^{-1}$  for most of the year but in several features stood out: lower salinity (less than  $34.6 \text{ g kg}^{-1}$ ) pulses occurred October 2004 and April 2005 and a maximum salinity of  $35.36 \text{ g kg}^{-1}$  at CP in January 2004. For ED, the semiannual variability was less than at CP and salinities were greatest in April, three months later than at ED. But minimums at ED occurred in August, one month before CP. For the data shown in Figure 6b, the maximum (minimum) salinity at ED was  $35.18 \text{ g kg}^{-1}$  ( $34.69 \text{ g kg}^{-1}$ ) in late February 2004 (late August 2005).

Note that the observed salinity profiles (Appendix A) were not monotonic due to the variability of Pacific and Gulf waters at each mooring site.

Figure 6c shows mean vertically averaged inflow time series. Here the biharmonic fits accounted for only 25% (11%) of the variability at CP (ED) and suggested stronger currents in summer, weaker in winter, and near zero (but no seasonal flow reversals) in October and April. Importantly, the character of the time series differed markedly from the temperature and salinity time series, especially at ED, where a series of oscillations associated with coastal trapped waves occurred; these oscillations are discussed below. At CP, these oscillations were weaker and less distinct. Flow reversal at CP was associated with low salinity water in October 2004 and the strongest outflow,  $-0.41 \text{ m s}^{-1}$  on 21 January 2006, was accompanied by moderate increases of temperature and salinity.

## COASTAL TRAPPED WAVES

The mean was removed from the pressure data which were then bandpass filtered to include only variability with periods between 20 and 80 days (Figure 6d). The ratio of mean pressure anomalies, ED/CP, was 7.3 and it was necessary to multiply the CP data shown in Figure 6d by ten so that the character and timing of the CP pressure anomalies is easily discerned. Most anomalies are likely intraseasonal coastal trapped waves (CTW). They occurred during May to November period indicating that they were caused by tropical storm landfall or gap wind events in southern Mexico or Costa Rica (Enfield and Allen, 1983; Spillane et al., 1987). In 2004, the three largest pressure anomalies at ED occurred about five days after peaks in sea level were observed at Manzanillo (located 690 km south of ED) (see Zamudio et al., 2008; Lavín et al. 2014). And similar but smaller peaks occurred about 5 days later at CP which is located about 1300 km from ED following a path along the continental shelf to the northern edge of San Pedro Martir Basin (this marks the beginning of the mid-Gulf region) and subsequently southward along the Gulf coast of Baja California (see Martínez and Allen 2004; Gutiérrez et al., 2014). These correspond to a phase speed of  $1.6 \text{ m s}^{-1}$  and  $3 \text{ m s}^{-1}$ , respectively. Note that the relationship with Manzanillo sea level was not observed in 2005 and 2006 possibly due to relocation of the Manzanillo tide gauge.

The maximum pressure anomaly at ED (CP) was 1.47 (0.17) dbar at 0155 on 12 June 2004 (1535 on 1 November 2004). Maximum correlation of pressure anomalies between ED and CP, 0.3, occurred when ED led CP by 4.9 days. A close examination of the relationship between the ED and CP pressure signals (Figure 6d) indicated that the anomalies were typically longer period when they reached CP. After August 2005, the relationship changed and waves appeared to be out of phase on either side of the Gulf.

The pressure anomalies often coincided with inflow oscillations and smaller amplitude oscillations in temperature and salinity. Observed kinematic relationships between the pressure and inflow and temperature were calculated for the 0.05-0.0125 cycles per day (20-to-80-day) band

following Merrifield (1992). Cross-correlation was used to determine the lag for largest magnitude correlation between time series and subsequently least squares regression was used to determine the relationship between the time series at that lag. Results are shown in Table 2. For results listed in Table 2, lags were less than 16 hours, correlations with velocity at ED (CP) were 0.54 (0.60) and yielded regressions of  $0.15 (-0.72) \text{ m s}^{-1} \text{ dbar}^{-1}$ . Time lags were similar for Conservative Temperature: correlations for ED (CP) were 0.19 (0.36) and regressions  $0.26 (5.4) \text{ }^{\circ}\text{C dbar}^{-1}$ . This indicated that CTW pressure anomalies were associated with increased flow and higher temperature as observed at mid-Gulf (Merrifield and Winant, 1989). Zamudio et al. (2008) used a numerical model to show that CTW can also strengthen the Mexican Coastal current in summer.

## SURFACE GEOSTROPHIC CURRENTS

Observations of temperature, salinity, and pressure from moorings were used to estimate the dynamic height anomaly,  $\Delta D$ , and steric height anomaly,  $h'$ , for each mooring (note  $h' = 10\Delta D/g$ ), where  $g$  is gravitational acceleration (Talley et al., 2011). The difference of steric height, ED – CP, is shown in Figure 7a, and compared with differences in satellite measurements of the height of the ocean surface at the two mooring locations. There was general agreement between the moored and satellite height differences for seasonal time scales. The higher frequency ( $\approx 3$  week period) oscillations were similar in amplitude and duration in part due to smoothing. CTW appear as positive oscillations as they were larger at ED than CP. Larger CTW in mid-June and November 2004 as well as July 2005 are easily discerned. But the satellite and moored oscillations coincided in only a few instances, e.g., February 2004 and August and September 2005. And there were instances where the difference between satellite and moored values were large; two examples are in December 2004 when the mooring data was  $-0.12 \text{ m}$  while the satellite height data were  $0.04 \text{ m}$  and in late fall 2005 when the rapidly declining satellite estimates led the mooring observations by about one to two months. This lack of agreement for higher frequencies is due, in part, to the nearly ten-day temporal

**Table 2.** Covariance between moored observations of bottom pressure and either alongshore velocity ( $V_r$ ), or conservative temperature ( $\Theta$ ), for the frequency band 0.05 to 0.0125 cpd. Here the maximum correlation ( $r$ ), and response,  $b$ , were observed at lag  $\tau$ . Average refers to the vertically averaged quantities shown in Figure 6.

<b>El Dorado</b>	<b>r</b>	<b><math>\tau</math>, hours</b>	<b>b</b>
$V_r$ vs pressure			$m (s \text{ dbar})^{-1}$
40	0.53	-1.5	0.17
80	0.53	0	0.15
108	0.48	-1.25	0.11
Average	0.54	1.5	0.15
$\Theta$ vs pressure			$^{\circ}C \text{ dbar}^{-1}$
40	-0.14	-1.5	
80	0.38	4.0	0.64
120	0.43	-0.5	
Average	0.19	3.2	0.26
<b>Cabo Pulmo</b>	<b>r</b>	<b><math>\tau</math>, hours</b>	<b>b</b>
$V_r$ vs pressure			$m (s \text{ dbar})^{-1}$
40	-0.54	0	-0.99
80	-0.62	-1.75	-0.85
120	0.14	16.25	0.04
Average	-0.60	-0.75	-0.72
$\Theta$ vs pressure			$^{\circ}C \text{ dbar}^{-1}$
40	0.32	3.6	8.33
80	0.37	3.1	5.16
120	0.39	3.65	2.83
Average	0.36	3.5	5.4

resolution of the satellite data (Valle-Rodríguez and Traslviña-Castro, 2017). The covariance (not shown) was maximum when the satellite data led the mooring data by one week; the correlation at this lag was  $0.64 \pm 0.04$ .

Figure 7b is a time series of the along-gulf wind stress averaged across Pescadero Basin; the data have been smoothed with a low pass filter with a three-week cutoff. Blue and red dots distinguish between poleward and equatorward winds, the former associated with the North American monsoon. The northwestward (southeastward) winds corresponded to periods when ED steric height was greater (less) than that at CP. The moored velocity data was conditionally sampled for mean currents during each wind regime (Figures 5a, b). At CP, the outflows reached  $\sim -18 \text{ cm s}^{-1}$  at 50 m and were about twice as strong between 35 m to 95 m during the monsoon than during southward winds. At ED, the current had maximum inflow of

$14 \text{ cm s}^{-1}$  at 35 m during the monsoon, about three times greater than the mean flow at 35 m during southward winds; but the mean monsoon current decreased with depth and was only about half the speed of the mean current for southward winds at 120 m.

Shorter period oscillations of wind stress agreed best with the steric height differences when CTW were absent. A good example of shorter period wind forcing effecting steric height difference was October through December, 2004, most notably when the strong equatorward winds (a late December storm) raised the sea level at CP by about 0.8 cm. Agreement was also good during the same period in 2005 when a tropical storm transits the entrance to the Gulf in early October (see Figure 9). The covariance between the moored steric height differences and the wind stress was maximum at zero lag and the correlation was 0.59. The biharmonic fits shown in Figure

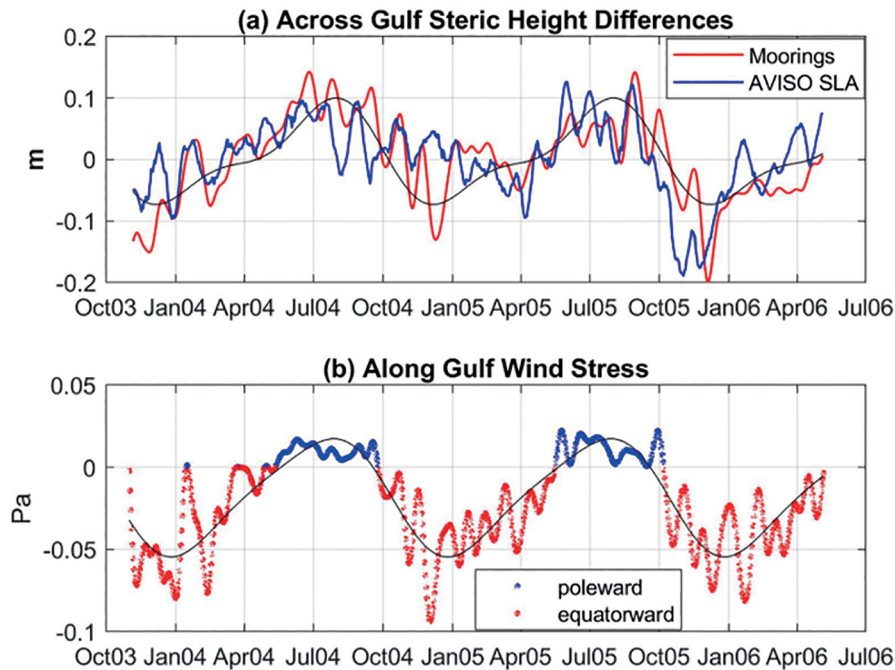


**Figure 7.** Surface geostrophic inflow and wind stress. (a) Smoothed time series of the difference of steric height between moored arrays (ED-CP) (red line) on either side of Pescadero Basin as well as the difference between satellite measured sea surface height at the mooring locations (blue line). Positive differences mean height is greater at ED than CP so geostrophic flow is directed into the Gulf. The black line is a biharmonic (annual, semiannual frequencies) fit to the moored steric height difference. (b) Mean wind stress across the Gulf between the two mooring locations. Blue dots correspond to poleward winds (the North American monsoon) and red dots correspond to equatorward winds. The black line is a least squares biharmonic (annual, semiannual frequencies) fit to the wind stress time series.

7 indicated that maximum wind stress (moored sea level difference) occurred on 1 August (29 July), the minimum on 27 Dec (7 Dec), with zero crossings on 21 May and 17 September (18 April and 1 October). Least squares fit for sea level difference  $\Delta_{SLD}$  (m) as a function of wind stress  $\tau_w$  (Pa) yielded  $\Delta_{SLD} = 0.56 \tau_w$  ( $\Delta_{SLD} = 0.11 \tau_w$ ) for poleward (equatorward) winds. The greater sensitivity of sea level difference to poleward winds is surprising given their lower wind stress and must be due to the head of the Gulf blocking the wind setup.

Differences in dynamic height anomaly between moorings can be used to estimate the mean geostrophic inflow,  $v_g$ ,  $V_g = \frac{(\Delta D_{ED} - \Delta D_{CP})}{fL}$ , where  $f$  is the Coriolis parameter and  $L$  is the distance between the two moorings, about 181 km. A difference in dynamic height anomaly of  $0.1 \text{ J kg}^{-1}$  (about the same as  $0.1 \text{ m}$  difference of steric height) across Pescadero Basin

corresponds to a mean geostrophic current of  $0.94 \text{ cm s}^{-1}$  or a mass transport for a  $1 \text{ m}$  thick layer of  $1.7 \text{ kt s}^{-1}$  into the Gulf. The altimeter measurements yielded geostrophic currents and transports for the ocean surface while the mooring dynamic height yields the transports at 20 dbar relative to 120 dbar. Note that the 2-year average of the mooring steric height (altimeter) difference is  $0.014 \text{ m}$  ( $-0.002 \text{ m}$ ) from 1 Jan 2004 to 1 Jan 2006 or  $0.010 \text{ m}$  ( $0.006 \text{ m}$ ) for 1 Apr 2004 to 1 Apr 2006.

### BALANCE OF MASS AND HEAT TRANSPORT BETWEEN SHELF MOORINGS

The mass and heat transport between the Gulf and the Pacific Ocean for the water columns at CP and ED is estimated. The observed flux at each mooring for each 15-minute sample was calculated. For CP, the mass transport,  $M^{CP}$ , was calculated from the 4-m binned velocity observations

between 20 m and 120 m,  $\Delta x$  is 1 m and  $\Delta z$  is 4 m (2 m) for depths from 116 to 24 m (120 and 20 m):

$$M^{CP}(t) = \sum_{i=1}^{26} V_i(t) \rho(t) \Delta x \Delta z$$

The Absolute Salinity and Conservative Temperature at depths 40, 80, and 120 m were smoothed to 15 minutes, interpolated to 4 m intervals between 120 and 20 m using the MATLAB pchip function and the density,  $\rho$ , calculated. At each 4 m level, the heat content was determined as  $hc_i = c_p^0 \rho_i(t) \Theta_i(t)$  where  $c_p^0$  is the specific heat,  $\Theta$  the Conservative Temperature and  $\rho$  the density. The heat flux,  $H^{CP}$ , is then determined as

$$M^{CP}(t) = \sum_{i=1}^{25} V_i(t) hc_i(t) \Delta x \Delta z$$

$M^{ED}$  and  $H^{ED}$  were determined using the same equations but with observations from mooring ED. An annual cycle was determined by averaging daily data by the year day.

The annual cycle of heat flux for both moorings is shown in Figure 8a. The annual mean and standard error for the heat flux was  $6.5 \times 10^8 \pm 1.9 \times 10^8 \text{ J s}^{-1}$  at ED and  $-5.8 \times 10^8 \pm 1.6 \times 10^8 \text{ J s}^{-1}$  at CP. There was a distinct seasonal pattern, with heat flux diverging to values which were larger (smaller) than their annual mean at ED (CP) for May 22 to September 7 and December 16 to February 2. For late spring-summer, the CP values decreased slightly from about  $-0.8 \times 10^9$  to  $-1.2 \times 10^9 \text{ J s}^{-1}$

while any trend at ED was obscured by large fluctuations associated with CTW passage. For winter, CP heat flux was minimum,  $-1.8 \times 10^9 \text{ J s}^{-1}$ , on January 18 while observed ED heat fluxes ranged from 0 to  $1 \times 10^9 \text{ J s}^{-1}$ . The annual pattern of mass transport resembled that of heat flux (Figure 8a).

It is not expected that the mass and heat fluxes observed at each mooring should balance one another as the pattern of flow between the moorings is highly variable, for example when mesoscale eddies (Castro et al., 2017) or filaments (Lavín et al., 2009) form. In fact, the balance of the fluxes at the mouth of the Gulf. The net heat flux for ED and CP was estimated as  $H(t) = H^{CP}(t) + H^{ED}(t)$ . The time integral of the net heat flux is shown in Figure 8b along with the corresponding integral for net mass transport. Downward (upward) slope with increasing time indicates net cooling (warming) or net outflow (inflow). The integral of these fluxes suggested that a pattern of yearly trends existed but changed at the end of the fall transition. Net cooling and outflow occurred from May through December 2004 while 2005 was a year of net heating and inflow. Net heat (mass) decreased to a minimum of  $-1.85 \times 10^{17} \text{ J}$  ( $-3.1 \times 10^9$  tonnes) on 11 December 2004 (after strong equatorward winds) and thence increased to a maximum on 29 December 2005 of  $1.6 \times 10^{17} \text{ J}$  ( $1.9 \times 10^9$ ).

The fall transitions are prominent in Figure 8b and were preceded by heat (mass) gains between

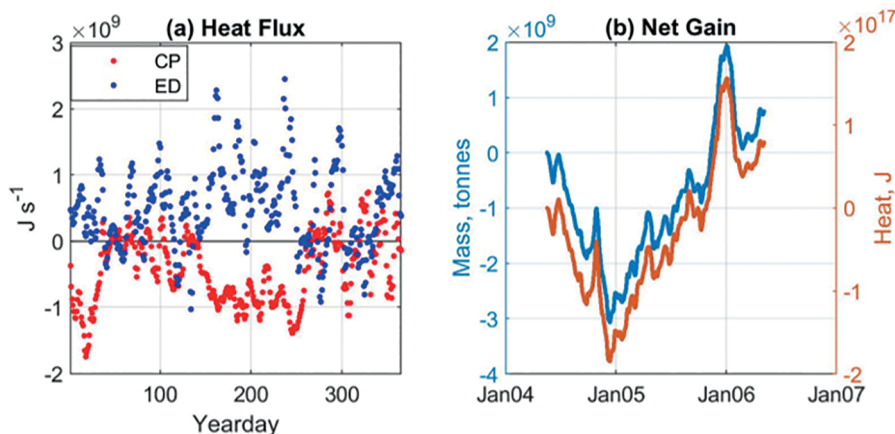


**Figure 8.** Temporal behavior moored fluxes. (a) Annual variability of heat flux. (b) Time integral for the sum of the mass transport (blue line) and heat flux (orange line) observed between 20 m and 120 m at the Cabo Pulmo and El Dorado moorings from 17 May 2004 to 5 May 2006.

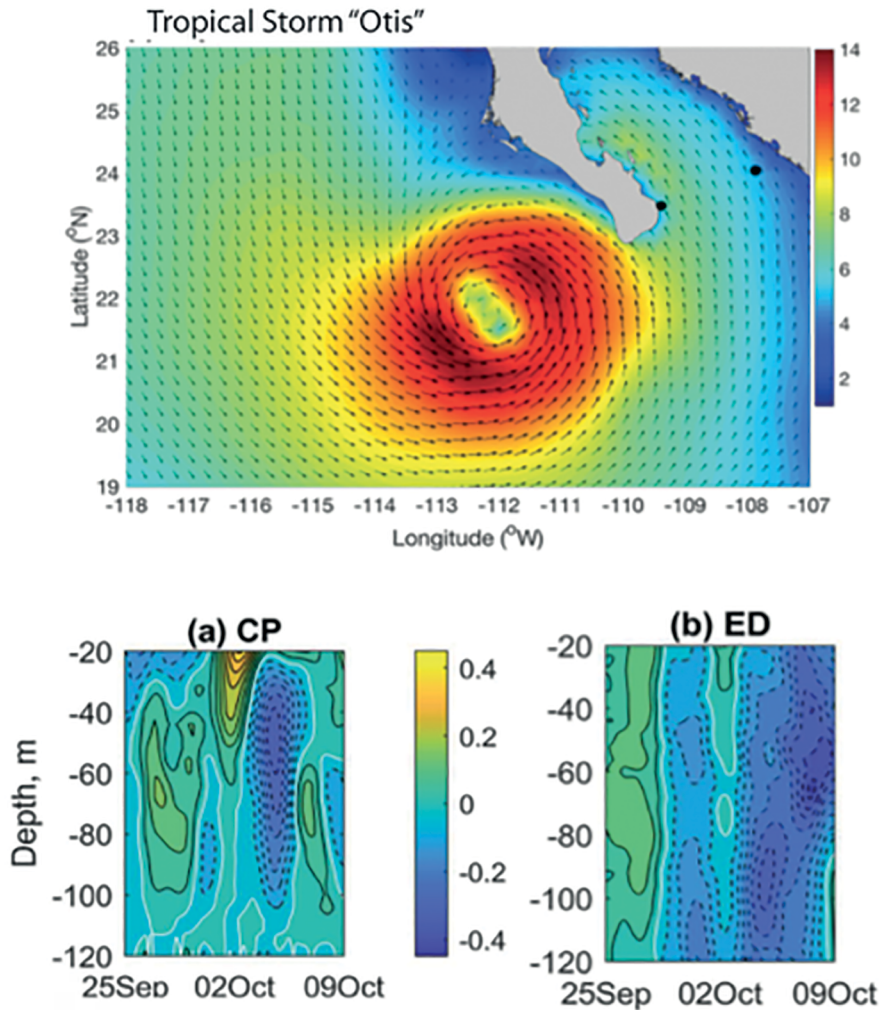


**Figure 9.** Impact of tropical storm Otis on Pescadero Basin. Upper panel illustrates the wind speed on October 1-2, 2005, obtained from ERA5 data. The color bar gives the wind speed in  $\text{m s}^{-1}$ , the wind direction is shown by arrows. The two black dots at the entrance of the Gulf show mooring locations, the Cabo Pulmo (CP) mooring next to the eastern tip of Baja California and the El Dorado (ED) mooring next to the mainland. Observed alongshore currents are shown for the period from 25 September to 9 October 2005; (a) Cabo Pulmo and (b) El Dorado. The color bar is the same for both figures and shows the current speed in  $\text{m s}^{-1}$ ; contours are shown at  $0.05 \text{ m s}^{-1}$  intervals with solid black lines indicating flow into the Gulf, dashed lines flow out of the Gulf, and the white contour is the zero isotach.

25 September and 27 October 2004 of  $7.7 \times 10^{16}$  J ( $9.0 \times 10^8$  tonnes) and followed by heat (mass) loss between 27 October and 11 December of  $-1.5 \times 10^{17}$  J ( $-2.1 \times 10^9$  tonnes). The fall transition in 2005 was delayed and preceded by a heat (mass) gain from 9 Oct 2005 to 2 January 2006 of  $1.83 \times 10^{17}$  J ( $2.84 \times 10^9$  tonnes) and followed by a heat (mass) loss from 2 January to 23 February of  $-1.19 \times 10^{17}$  J ( $-1.80 \times 10^9$  tonnes). At the end of the two-year period, the mass had increased  $7.5$

$\times 10^8$  tonnes and the net heat gain  $8.0 \times 10^{16}$  J. The yearlong persistence of trends is surprising although in early 2006 the heat continued to gain after the fall transition, unlike the reversal seen in 2004.

CTW wave features were seen in both time series shown in Figure 8. For Figure 8a, the heating at ED included nine to ten spikes of heat flux greater than  $1 \times 10^9 \text{ J s}^{-1}$ , about the same number of ED pressure anomalies were greater than 0.4

dbar. The largest 2004 ED pressure anomaly at ED occurred in June and its heat and mass flux are discussed below (Figure 10).

## RESPONSE TO TROPICAL STORMS

The effect of tropical storms on circulation in Pescadero Basin has been well documented for Hurricane *Juliette* which moved across mouth of the Gulf on 27-30 September 2001 (Zamudio et al., 2010). Here we confirm results of Zamudio et al., *ibid*. Only one tropical storm moved across the Gulf entrance when shelf moorings CP and ED were in place: tropical storm *Otis*, the last tropical storm of 2005, moved across the Gulf entrance from 28 September to 5 October (Figure 9). *Otis* was not as strong as *Juliette* and was about 50 km further to the west but the seasonal northward winds in PB were strengthened to about  $8 \text{ m s}^{-1}$  along the BCS coast. Velocity data for CP are shown in Figure 9a and indicate that inflow in the upper 60 m accelerated to  $0.4 \text{ m s}^{-1}$  on 2 October, subsequently relaxing with  $-0.4 \text{ m s}^{-1}$  outflow on 3-4 October. At ED (Figure 9b), the flows were similar to CP but much weaker: the inflow on 2 October was only  $0.1 \text{ m s}^{-1}$ . As noted above, about a week later the temperatures at both CP and ED begin a sharp decrease from  $18^\circ\text{C}$  to  $15^\circ\text{C}$ , indicating the presence of Pacific waters. It is interesting to speculate that the subsequent warming at CP to  $>20^\circ\text{C}$  in early December (Figure 6a) was the result of northern Gulf waters being blocked by *Otis*

during its transit of the mid-Gulf and thence delayed at reaching CP.

The effects of a third tropical storm were observed in 1995 when *Flossie* (10-11 August 1995) (Castro et al., 2006) moved across the Gulf entrance immediately before cruise P07. Upwelling along BCS and convergence and downwelling along Sinaloa were observed for PB sections occupied between 12-15 August 2005.

## DISCUSSION

To balance the mass transport for the PB section, it was necessary to add barotropic flows that ranged from  $-1.14$  for station 2 near the BCS coast to  $-0.18 \text{ cm s}^{-1}$  at station 6 (located on the western flank of Alarcon Seamount; Figure 1). This kept the position of the zero isotach at  $108.72^\circ\text{W}$  (Figure 4d), dividing inflow to the Gulf on the east from flow out of the Gulf to the west. The magnitudes of the adjusted velocities were similar to those observed by the mooring on the shelf of BCS. The net mass flux for this section was  $4.7 \text{ kt s}^{-1}$  ( $1 \text{ kt} = 1 \times 10^6 \text{ kg}$ ) which balanced the freshwater budget for the Gulf. The net heat flux for the section was  $5.3 \times 10^{12} \text{ J s}^{-1}$ , much greater than the  $-18.4 \times 10^{12} \text{ J s}^{-1}$  observed by Castro et al. (1994). Lavín et al. (2009) found good agreement between heat flux estimates using geostrophic and directly measured currents in 7-17 June 2004 at the entrance to the Gulf but his estimate of heat flux,  $121 \times 10^{12} \text{ J s}^{-1}$ , was five times greater than the  $21 \times 10^{12} \text{ J s}^{-1}$

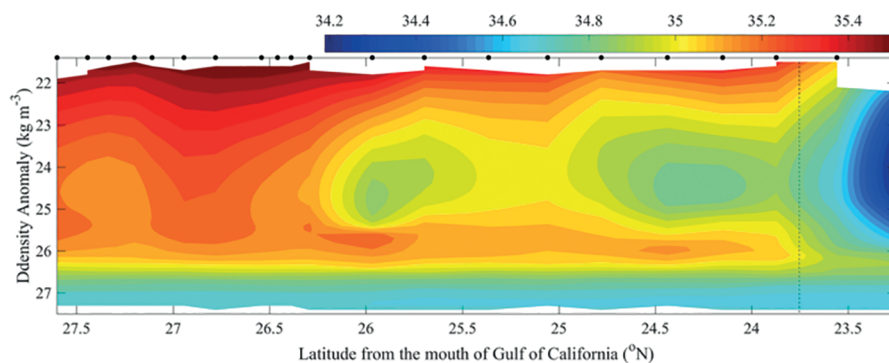


**Figure 10.** Section of Absolute Salinity ( $\text{g kg}^{-1}$ ) on isopycnals along the western boundary of the Gulf of California. Observations were collected in August 2004 by the NAME experiment (see Lavín et al., 2013). The color bar next to the upper abscissa shows salinity values. The vertical black dash line shows the location of the PB section. Black dots along the upper abscissa indicate the location of hydrographic stations.

$s^{-1}$  estimated by Castro et al. (1994). Lavín et al. (2009) attributes this difference to the unusual synoptic conditions during 7-17 June. There is no similar explanation for the difference in our estimate and Castro et al. (1994); assimilation of the ship-board data used here and that used by Castro et al. (ibid) with a numerical model might resolve this issue (see Zamudio et al., 2008).

The structure of the mean Absolute Salinity field is best shown along isopycnals (Figure 4c) as isohalines tend to be parallel to isopycnals. The isopycnal coordinates also stretch the view of the subsurface lens of  $34.8 \text{ g kg}^{-1}$  Pacific water centered along the  $24.8 \text{ kg m}^{-3}$  isopycnal (Figure 4d); these low salinity waters flow into the Gulf on the eastern (Sinaloa) side of the PB section at about 55 dbar depth. Next to BCS, salinities greater than  $34.95 \text{ g kg}^{-1}$  extended across isopycnals from near the surface,  $23 \text{ kg m}^{-3}$ , to  $26.2 \text{ kg m}^{-3}$  and were advected out of the Gulf. The outflow on the deeper  $26 \text{ kg m}^{-3}$  isopycnal suggests overturning of high salinity waters in the Gulf (Bray, 1988, and López et al., 2008). This connection is shown in Figure 10 as high salinity plume along the  $26 \text{ kg m}^{-3}$  isopycnal from the mid-Gulf region to the PB section along the BCS side of the Gulf. The two Pacific Ocean stations at the mouth of the Gulf appear as a low salinity barrier, especially for high salinity surface waters extending along the  $22 \text{ kg m}^{-3}$  isopycnal. The Gulf surface waters may recycle back into the Gulf (as shown near the center of the PB section (Figure 3b, d) or move into the Pacific inshore (Figures 3b, d) (Collins et al., 2015; Castro et al., 2017; Muñoz-Larios et al., 2022). The deeper Gulf outflow should join poleward flows along BCS (Pl. 2, C. Castro et al., 2001; Gómez-Valdivia et al., 2017; Valle-Rodríguez and Trasviña, 2017), adding salinity, heat and decreasing the oxygen for these waters.

Moorings were used to measure the mass and heat flux directly as well as the near surface along Gulf flow between the moorings. The yearly data (Figure 8a) showed two periods, May 22 to September 7 and December 16 to February 2, when the inflow of heat at ED was persistently balanced by outflow at CP; at other times, the heat flux at the two moorings reversed or, in some instances, the flux was oriented in the same direction.

The biharmonic fit for the 20 m across gulf geostrophic velocity (Figure 7a) was similar to that for temperature (Figure 6a) and wind stress (Figure 7b) with maximum (minimum) inflow in August (December) which reached about  $0.01 \text{ m s}^{-1}$  ( $-0.01 \text{ m s}^{-1}$ ). An interesting effect of the fall wind reversal was that equatorward winds transported water toward BCS (Ekman transport) and southward (wind setup). Subsequently, the temperatures at CP increased due to advection of GCW around BCS.

This meant that the dynamic height at CP exceeded that of cooling waters at ED, assuring that the outflow of GCW waters received a boost from near surface geostrophic outflow. With respect to temperature, a similar situation did not occur in spring as the transition was marked by the onset of poleward winds and temperatures of the Gulf waters that moved around BCS warmed at nearly the same rate as those at ED (Figure 6a). These fall vs summer temperature differences explain why fall heat flux observed by Castro et al. (1994), was twice that observed in spring. But the two spring transitions did mark freshening of ED waters, consistent with the Lavín et al. (2009) observations.

The salinity of shallow ( $<50 \text{ m}$ ) waters in the region immediately south of the Gulf (from the Mexican coast to  $110^\circ\text{W}$  between  $16^\circ\text{N}$  to  $22.8^\circ\text{N}$ ) increases from April through June (Fig. 3b, Portela et al., 2016). The only regional source for the salinity increase is GCW. The predominant poleward flow observed at ED (Figure 8a above) during year days 91 to 182 raise the issue of how GCW gets to the south. Figure 5b suggests the wind-driven surface layer at ED moves southward: the mean flow above 25 m during April to 21 May is weak ( $-0.02 \text{ m s}^{-1}$ ) equatorward flow. A more regional view of surface circulation (Fig. 18a, Valverde-Kalish, 2016) shows spring (March through May) surface geostrophic flow for the region using ADT data from 1993 to 2013. The Valverde-Kalish (2016) chart indicated southward flow  $\approx 0.1 \text{ m s}^{-1}$  from the western ( $109^\circ\text{W}$ ) side of the Gulf which turns eastward at  $20^\circ\text{N}$  and thence southward along the Mexican coast. In summer (ibid, Fig. 18b) the ADT data indicated poleward flow along the Mexican coast into the Gulf, in agreement with the ED measurements shown

above in Fig. 8. A more rigorous study of the spring freshwater balance is warranted.

Spikes of heat and mass flux about one month in duration appeared in Figures 7 and 8; most of these spikes appear related to CTW passage at ED, especially in 2004 (Figure 6d). In 2004, the temperatures at the moorings were observed to slowly increase from the winter minimum in May (Figure 6a) and, at ED, warming was observed to accelerate at the end of May, about the same time as a CTW was observed at both ED and CP. The heat flux at each mooring during 20 May to 1 July 2004 is shown in Figure 11. For ED (Figure 11b), the heat flux changed from negative to positive on 30 May for the upper 60 m and the positive heat flux deepened to 120 m on 6 June. The CTW crested at 1.45 dbar at 0400 on 11 June (marked by a vertical red line on Figure 11b), two days after the maximum vertically integrated heat flux,  $4.7 \times 10^9 \text{ J s}^{-1}$ , at 0200 9 June 2004. Subsequent peaks of heat flux associated with CTW passage occurred 4 and 10 days later. On 27 June the flow reversed at

ED marking the end of the CTW event at ED; the total heat transported into the Gulf was  $4.73 \times 10^{15} \text{ J}$ .

At CP, a small pressure peak was observed at 0700 16 June, about six days after the CTW crest passed ED (Figure 6d). From 20 May to 1 July, a small amount of heat flux at CP was directed into the Gulf between 20 and 40 m (Figure 11a). The heat flux for most of the rest of the water column was directed into the Pacific Ocean. The largest vertically integrated outflow,  $-1.9 \times 10^9 \text{ J s}^{-1}$ , occurred at 0600 10 June (a day after the maximum inflow at ED) and the associated pressure peak, 0.052 dbar, was observed six days later at 0700 16 June. The CP outflow sum over the 30 May to 27 July was  $-2.86 \times 10^{15} \text{ J}$ .

The moorings measured a mean June heat flux of  $1.4 \times 10^7 \text{ J s}^{-1}$  at ED and  $-1.1 \times 10^7 \text{ J s}^{-1}$  at CP or a net of  $0.4 \times 10^7 \text{ J s}^{-1}$  for a 2 m length  $\times$  1 m width  $\times$  100 m depth column of water. This flux is compared with the Castro et al. (1994) estimate of heat flux across the mouth of the Gulf in June, 14

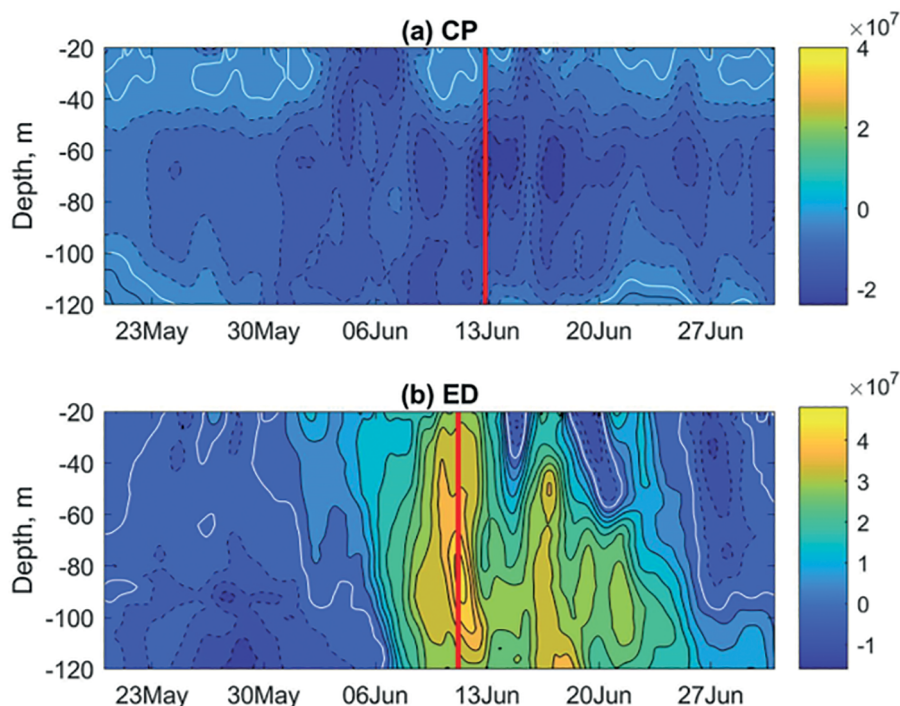


**Figure 11.** Alongshore heat flux at moorings during CTW passage in Spring 2004. Contour intervals are  $0.4 \times 10^7 \text{ J s}^{-1}$ , dashed contours indicate flow out of the Gulf, solid contours the flow into the Gulf, and the white contour is the zero isotach. Vertical red lines mark the peak of observed CTW at each location. Current and temperature data shown here have been smoothed with a 2-day filter to remove diurnal tides. Color bars have same range but colors represent different values. (a) CP mooring site. (b) ED mooring site.

$\times 10^{12} \text{ J s}^{-1}$ . The Castro et al. (ibid) estimate was for slab 400 m in depth which extended across the mouth of the Gulf. Assuming that this heat flux is distributed uniformly through the water column, then dividing by the (width of the Gulf  $\times$  four) yields  $2 \times 10^7 \text{ J s}^{-1}$  for a one square meter water column which is 100 m deep. The mooring heat flux,  $0.2 \times 10^7 \text{ J s}^{-1}$  (a volume of a one square meter column which is 100 m deep) was a tenth of the climatological heat flux. A conclusion is that the heat fluxes observed by the coastal moorings were not representative of the across gulf transport derived by Castro et al. (ibid).

It is also disappointing that the moorings did not detect flow events associated with deep jets that occur in deeper waters. For example, Roden (1972) observed a 30 km wide jet with  $-0.5 \text{ m s}^{-1}$  currents at the surface and  $-0.4 \text{ m s}^{-1}$  at 600 m next to BCS on 5-6 December 1969. Collins et al. (1997) observed similar deep jets on either sides of the Gulf on 2-4 May 1992. The broad shelf and subsurface ridge off Sinaloa (Figure 1) might have isolated the ED mooring from these events but the CP mooring is well within the 35 km Rossby radius of the jets observed next to BCS. Note too that a filament of CCW observed by Lavín et al. (2009) in June 2004 did not appear to affect the moored observations.

Ripa (1997) has indicated that the circulation at the mouth of the Gulf is key to determining and understanding the flow within the Gulf so efforts to observe these flows should continue. New higher resolution satellite altimeter data will help in determining the details of surface circulation, but direct observation of the flows is needed to sort out important kinematic details, e.g., baroclinic vs barotropic flow, forcing of deep jets, paths and causes of CTWs. Bottom pressure measurements on Alcarón Seamount and similar depths at either coast would detect deep jets. Velocity observations could be accomplished by instrumenting ferries that sail daily between Mazatlán and La Paz (and vice versa) with vessel mounted ADCPs and GPS receivers that measure the ship's attitude. An example of a successful program of this type are the *MV Oleander* measurements of the Gulf Stream (Flagg et al., 1998). An alternative would be to use ocean gliders. Gliders are now routinely

deployed by academic laboratories and have demonstrated that they are able to observe strong flows including the Gulf Stream (Heiderich & Todd, 2020).

## ACKNOWLEDGMENTS

This was a joint project between the Naval Postgraduate School and the University Autónoma de Baja California. It has been sponsored by the National Science Foundation (NSF), Consejo Nacional de Ciencia y Tecnología (CONACyT), the Naval Oceanographic Office, the Oceanographer of the Navy, the Secretaría de Marina de Mexico and Universidad Autónoma de Baja California. Reginaldo Durazo, Tarry Rago, Marla Stone, Rafael Blanco, Sergio Larios, Eduardo Gil, Luis F. Navarro, and Newell Garfield aided in data collection and processing. We could not have made these measurements without the assistance of the officers and crews of the research vessels listed in Table 1. Data from NAME0408 were obtained as part of the North American Monsoon Experiment (NOAA-GC04-219) and CICESE-UABC collaboration. Bathymetry data were obtained from GEBCO Compilation Group (2021) GEBCO 2021 Grid (doi:10.5285/c6612cbe-50b3-0cff-e053-6c86abc09f8f).

We also thank two anonymous reviewers for comments that greatly improved this manuscript.

(RC, CAC) Affonso Mascarenhas was responsible for Mexican participation in this project including support for shipboard measurements and purchase of instrumentation for the El Dorado mooring. He completed an initial analysis of the moored data in January 2007 and it has taken the other two authors 15 years to complete the work.

(CAC) I was very fortunate to meet and work with Affonso and have many fond memories of the experiences that we shared. One that comes to mind is a cruise on the *B/O Alejandro Humboldt*. Oceanographers stood watch in a lab that was just abaft of the bridge on the boat deck. Affonso had an afternoon watch and at exactly 1400 the ship's captain would deliver Affonso a glass of rum and coke with ice. A navy tradition extended to the chief scientist, and certainly a well-deserved perk for running the cruise so well. Affonso's accomplishments on the cruise were too many to list but

included tying a perfect square knot in the hydro wire while the CTD was about 500 m deep.

(RC) We will always remember Affonso for his enthusiasm and good humor, especially his teaching of Physical Oceanography at UABC, his vision submitting Research projects, and interesting conversations of everyday life.

## AUTHOR CONTRIBUTIONS

C.A.C., R.C.: Data collection, Processing, Analysis, Project management

## REFERENCES

- ATLAS, R., HOFFMAN, N. R., ARDIZZONE, J., LEIDNER, S. M., JUSEM, J. C., SMITH, D. K. & GOMBOS, D. 2011. A cross-calibrated multi-platform ocean surface wind velocity for meteorological and oceanographic applications. *Bulletin American Meteorological Society*, 92(2), 157-174, DOI: <https://doi.org/10.1175/2010BAMS2946.1>
- BACON, S. & FOFONOFF, N. 1996. Oceanic heat flux calculation. *Journal of Atmospheric and Oceanic Technology*, 13(6), 1327-1329.
- BERON-VERA, F. J. & RIPA, P. 2000. Three-dimensional aspects of the seasonal heat balance in the Gulf of California. *Journal Geophysical Research*, 105(C5), 441-457, DOI: <https://doi.org/10.1029/2000JC900038>
- BORDONI, S., CIESIELSKI, P. E., JOHNSON, R. H., MCNOLDY, B. D. & STEVENS, B. 2004. The low-level circulation of the North American Monsoon as revealed by QuikSCAT. *Geophysical Research Letters*, 31(10), 2-5, DOI: <https://doi.org/10.1029/2004GL020009>
- BRAY, N. A. 1988. Water mass formation in the Gulf of California. *Journal of Geophysical Research*, 93(C8), 9223-9240.
- CASTRO, C. G., CHAVEZ F. P. & COLLINS, C. A. 2001. Role of the California undercurrent in the export of denitrified waters from the eastern tropical North Pacific. *Global Biogeochemical Cycles*, 15(4), pp. 819-830.
- CASTRO, R., LAVÍN, M. F. & RIPA, P. 1994. Seasonal heat balance in the Gulf of California. *Journal of Geophysical Research*, 99(C2), 3249-3261, DOI: <https://doi.org/10.1029/93JC02861>
- CASTRO, R., COLLINS, C. A., RAGO, T. A., MARGOLINA, T. & NAVARRO-OLACHE, L. F. 2017. Currents, transports, and thermohaline variability at the entrance to the Gulf of California (19-21 April 2013). *Ciencias Marinas*, 43(3), 173-190, DOI: <https://doi.org/10.7773/cm.v43i3.2771>
- CASTRO, R., DURAZO, R., MASCARENHAS, A., COLLINS, C. A. & TRASVIÑA, A. 2006. Thermohaline variability and geostrophic circulation in the southern portion of the Gulf of California. *Deep Sea Research I*, 53(1), 188-200, DOI: <https://doi.org/10.1016/j.dsr.2005.09.010>
- CASTRO, R., MASCARENHAS, A. S., DURAZO, R. & COLLINS, C. A. 2000. Seasonal variation of the temperature and salinity at the entrance to the Gulf of California, Mexico. *Ciencias Marinas*, 26(4), 561-583, DOI: <https://doi.org/10.7773/cm.v26i4.621>
- CHELTON, D. B. 1984. Seasonal variability of alongshore geostrophic velocity off central California. *Journal of Geophysical Research*, 89(C3), 3473-3486.
- CHELTON, D. B., DESZOEKE, R. A., SCHLAX, M. G., EL NAGGAR, K. & SIWERTZ, N. 1998. Geographical Variability of the First Baroclinic Rossby Radius of Deformation. *Journal of Physical Oceanography*, 28(3), 433-460. DOI: [https://doi.org/10.1175/1520-0485\(1998\)028<0433:GVOTFB>2.0.CO;2](https://doi.org/10.1175/1520-0485(1998)028<0433:GVOTFB>2.0.CO;2)
- CHRISTENSEN, N., DE LA PAZ, R. & GUTIERREZ, F. 1983. A study of sub-inertial waves off the west coast of Mexico. *Deep-Sea Research*, 30(8A), 835-850.
- COLLINS, C. A., CASTRO, R. & MASCARENHAS, A. 2015. Properties of upper ocean fronts associated with water mass boundaries at the entrance to the Gulf of California, November 2004. *Deep-Sea Research II*, 119, 48-60, DOI: <https://doi.org/10.1016/j.dsr2.2014.06.002>
- COLLINS, C. A., GARFIELD, N., MASCARENHAS, A., SPEARMAN, M. & RAGO, T. A. 1997. Ocean currents across the entrance to the Gulf of California. *Journal of Geophysical Research: Oceans*, 102(C9), 20927-20936, DOI: <https://doi.org/10.1029/97JC01302>
- ENFIELD, D. B. & ALLEN, J. S. 1983. The generation and propagation of sea level variability along the Pacific Coast of Mexico. *Journal Physical Oceanography*, 13(6), 1012-1033, DOI: [https://doi.org/10.1175/1520-0485\(1983\)013<1012:TGAPOS>2.0.CO;2](https://doi.org/10.1175/1520-0485(1983)013<1012:TGAPOS>2.0.CO;2)
- FLAGG, C. N., SCHWARTZ, G., GOTTLIEB, E. & ROSSBY, T. 1998. Operating an acoustic Doppler current profiler aboard a container vessel. *Journal of Atmospheric and Oceanic Technology*, 15, 257-271, DOI: [https://doi.org/10.1175/1520-0426\(1998\)015%3C0257:OADC%3E2.0.CO;2](https://doi.org/10.1175/1520-0426(1998)015%3C0257:OADC%3E2.0.CO;2)
- GUTIÉRREZ, M. O., LÓPEZ, M., CANDELA, J., CASTRO, R., MASCARENHAS, A. & COLLINS, C. A. 2014. Effect of coastal-trapped waves and wind on currents and transport in the Gulf of California. *Journal of Geophysical Research*, 119(8), 5123-5139, DOI: <https://doi.org/10.1002/2013JC009538>
- GÓMEZ-VALDIVIA, F., PARÉS-SIERRA, A. & FLORES-MORALES, A. L. 2017. Semiannual variability of the California Undercurrent along the Southern California Current System: A tropical generated phenomenon. *Journal of Geophysical Research: Oceans*, 122(2), 1574-1589.
- HEIDERICH, J. & TODD, R. E. 2020. Along-stream evolution of Gulf Stream volume transport. *Journal of Physical Oceanography*, 50(8), 2251-2270, DOI: <https://doi.org/10.1175/JPO-D-19-0303.1>
- IOC (Intergovernmental Oceanographic Commission), SCOR & IAPSO (International Association for the Physical Sciences of the Oceans). 2010. *Manual and Guides No. 56: The international thermodynamic equation of seawater-2010: calculation and use of thermodynamic properties*. Paris: UNESCO/SCOR/IAPSO.

- LARIOS-MUÑOZ, M., GONZÁLEZ-SILVERA, A., CASTRO, R., SANTAMARÍA-DEL-ÁNGEL, E. & LÓPEZ-CALDERÓN, J. M. 2002. Variability of hydrographic factors, biomass and structure of the phytoplankton community at the entrance to the Gulf of California (spring 2013). *Continental Shelf Research*, 235, 104665, DOI: <https://doi.org/10.1016/j.csr.2022.104665>
- LAVÍN, M. F., BEIER, E., GÓMEZ-VALDÉS, J., GODÍNEZ, V. M. & GARCÍA, J. 2006. On the summer poleward coastal current off SW México. *Geophysical Research Letters*, 33(2), L02601, DOI: <https://doi.org/10.1029/2005GL024686>
- LAVÍN, M. F., CASTRO, R., BEIER, E. & GODÍNEZ, V. M. 2013. Mesoscale eddies in the southern Gulf of California during summer: characteristics and interaction with the wind stress. *Journal of Geophysical Research: Oceans*, 118(3), 1367-1381, DOI: <https://doi.org/10.1002/jgrc.20132>
- LAVÍN, M. F., CASTRO, R., BEIER, E., CABRERA, C., GODÍNEZ, V. M. & AMADOR-BUENROSTRO, A. 2014. Surface circulation in the Gulf of California in summer from surface drifters and satellite images (2004-2006). *Journal of Geophysical Research Oceans*, 119(7), 4278-4290, DOI: <https://doi.org/10.1002/2013JC009345>
- LAVÍN, M. F., CASTRO, R., BEIER, E., GODÍNEZ, V. M., AMADOR, A. & GUEST, P. 2009. SST, thermohaline structure and circulation in the southern Gulf of California in June 2004, during the North American Monsoon Experiment. *Journal Geophysical Research*, 114(C2), C02025, DOI: <https://doi.org/10.1029/2008JC004896>
- LAVÍN, M. F. & MARINONE, S. G. 2003. An overview of the physical oceanography of the Gulf of California. In: VELASCO, O. U., SHEINBAUM, J. & OCHOA, J. (eds.). *Nonlinear processes in geophysical fluid dynamics*. New York: Springer, pp. 173-204, DOI: [https://doi.org/10.1007/978-94-010-0074-1\\_11](https://doi.org/10.1007/978-94-010-0074-1_11)
- LÓPEZ, M., CANDELA, J. & GARCÍA, J. 2008. Two overflows in the Northern Gulf of California. *Journal Geophysical Research Oceans*, 113(C8), C08023, DOI: <https://doi.org/10.1029/2007JC004575>
- LÓPEZ, M., FLORES-MATEOS, L. & CANDELA, J. 2021. Tidal currents at the sills of the Northern Gulf of California. *Continental Shelf Research*, 227, 104513, DOI: <https://doi.org/10.1016/j.csr.2021.104513>
- MARINONE, S. G., PARÉS-SIERRA, A., CASTRO, R. & MASCARENHAS, A. 2004. Correction to "Temporal and Spatial variation of the surface winds in the Gulf of California." *Geophysical Research Letters*, 31(10), L10305, DOI: <https://doi.org/10.1029/2004GL020064>
- MARTINEZ, J. A. & ALLEN, J. S. 2004. A modeling study of coastal-trapped wave propagation in the Gulf of California: Response to remote forcing. *Journal Physical Oceanography*, 34(6), 1313-1331, DOI: [https://doi.org/10.1175/1520-0485\(2004\)034<1313:AMSOCW>2.0.CO;2](https://doi.org/10.1175/1520-0485(2004)034<1313:AMSOCW>2.0.CO;2)
- MASCARENHAS, A. S., CASTRO, R., COLLINS, C. A. & DURAZO, R. 2004. Seasonal variation of geostrophic velocity and heat flux at the entrance to the Gulf of California, Mexico. *Journal Geophysical Research: Oceans*, 109(C7), C07008, DOI: <https://doi.org/10.1029/2003JC002124>
- MERRIFIELD, M. A. 1992. A comparison of long coastal-trapped wave theory with remote storm generation wave events in the Gulf of California. *Journal Physical Oceanography*, 22(1), 5-18.
- MERRIFIELD, M. A. & WINANT, C. D. 1989. Shelf circulation in the Gulf of California: a description of the variability. *Journal Geophysical Research*, 94(C12), 18133-18160.
- MUNK, W. 1950. On the wind-driven ocean circulation. *Journal Meteorology*, 7(2), 79-93.
- PADUAN, J. B., ZIERENBERG, R. A., CLAGUE, D. A., SPELZ, R. M., CARESS, D. W., TRONI, G., THOMAS, H., GLESSNER, J., LILLEY, M. D., LORENSON, T., LUPTON, J., NEUMANN, F., SANTA ROSA DEL-RIO, M. A. & WHEAT, C. G. 2018. Discovery of hydrothermal vent fields on Alarcón Rise and in Southern Pescadero Basin, Gulf of California. *Geochemistry, Geophysics, Geosystems*, 19(12), 4788-4819, DOI: <https://doi.org/10.1029/2018GC007771>
- PASCALE, S., BOOS, W., BORDONI, S., DELWORTH, T. L., KAPNICK, S. B., MURAKAMI, H., VECCHI, G. A. & ZHANG, W. 2017. Weakening of the North American monsoon with global warming. *Nature Climate Change*, 7, 806-812, DOI: <https://doi.org/10.1038/nclimate3412>
- PORTELA, E., BEIER, E., BARTON, E. D., CASTRO, R., GODÍNEZ, V., FIELDLER, P., PALACIOS-HERNÁNDEZ, E., SÁNCHEZ-VELASCO, L. & TRASVIÑA, A. 2016. Water masses and circulation in the tropical Pacific off central Mexico and surrounding areas. *Journal of Physical Oceanography*, 46(10), 3069-3081, DOI: <https://doi.org/10.1175/JPO-D-16-0068.1>
- RIPA, P. 1997. Toward a physical explanation of the seasonal dynamics and thermodynamics of the Gulf of California. *Journal of Physical Oceanography*, 27(5), 597-614.
- RODEN, G. I. 1972. Thermohaline structure and baroclinic flow across the Gulf of California entrance and in the Revilla Gigedo Islands region. *Journal Physical Oceanography*, 2(2), 1777-1803.
- RODEN, G. I. & GROVES, G. W. 1959. Recent oceanographic investigations in the Gulf of California. *Journal Marine Research*, 18(1), 10-35.
- ROSAS-VILLEGAS, F., LÓPEZ, M. & CANDELA, J. 2018. Currents and mixing the San Lorenzo overflow, Northern Gulf of California. *Journal of Geophysical Research: Oceans*, 123(2), 1339-1353, DOI: <https://doi.org/10.1002/2017JC0132>
- SIMPSON, J. H., SOUZA, A. J. & LAVÍN, M. F. 1994. Tidal mixing in the Gulf of California. In: BEVEN, K. J., CHATWIN, P. C. & MILLBANK, J. H. (eds.). *Mixing and transport in the environment*. New York: John Wiley & Sons, pp. 169-182.
- SPEARMAN, M. G. 1993. *Water masses and the thermohaline circulation at the entrance to the Gulf of California*. MSc. Monterey: Naval Postgraduate School.
- SPILLANE, M. C., ENFIELD, D. B. & ALLEN, J. S. 1987. Intraseasonal oscillations in sea level along the west coast of the Americas. *Journal Physical Oceanography*, 17, 303-325.

- STEVENSON, M. R. 1970. On the physical and biological oceanography at the entrance of the Gulf of California, October 1966-August 1967. *Bulletin International American Tropical Tuna Commission*, 14(3), 389-504.
- SVERDRUP, H. U. 1939. The Gulf of California: preliminary discussion of the cruise of the "E.W. Scripps" in February and March 1939. In: *Proceedings of the Sixth Pacific Science Congress. Volume III*. Berkeley, Stanford and San Francisco, July 24 to August 12, 1939. San Francisco: PSC, pp. 1-7.
- TALLEY, L. D., PICKARD, G. L., EMERY, W. J. & SWIFT, J. H. 2001. Descriptive physical oceanography: an introduction. Boston: Elsevier.
- TORRES-OROZCO, E. 1993. *Volumetric analysis of the water masses of the Gulf of California*. MSc. Baja California: Centro de Investigación Científica y de Educación Superior de Ensenada.
- TRENBERTH, K. E., LARGE, W. G. & OLSON, J. G. 1990. The mean annual cycle in global ocean wind stress. *Journal Physical Oceanography*, 20(11), 1742-1760.
- VALLE-RODRIGUEZ, J. & TRASVIÑA-CASTRO, A. 2017. Poleward currents from coastal altimetry: The west coast of Southern Baja California, Mexico. *Advances in Space Research*, 59(9), 2313-2324, DOI: <http://dx.doi.org/10.1016/j.asr.2017.01.050>
- VALVERDE-KALISEH, C. A. 2016. *Characterization of ocean circulation at the entrance to the Gulf of California*. MSc. Baja California: Universidad Autónoma de Baja California.
- WARSH, C. E. & WARSH, K. L. 1971. Water exchange at the mouth of the Gulf of California. *Journal Geophysical Research*, 76(33), 8098-8106.
- ZAMUDIO, L., HOGAN, P. & METZGER, E. J. 2008. Summer generation of the Southern Gulf of California eddy train. *Journal of Geophysical Research: Oceans*, 113(C6), C06020, DOI: <https://doi.org/10.1029/2007JC004467>

## APPENDIX A. MOORED SALINITY TIME SERIES

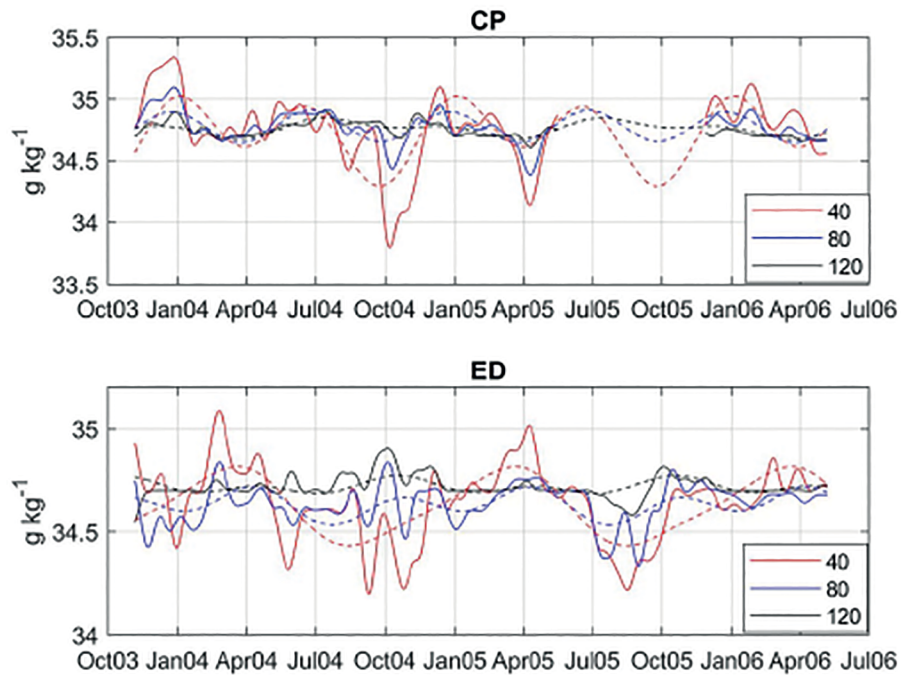


**Figure A1.** Moored salinity time series at 40, 80, 120 m depth (solid lines) and biharmonic fit (dashed lines). (upper) Cabo Pulmo. (lower) El Dorado. Note that the range of the ordinate at Cabo Pulmo is 0.8  $\text{g kg}^{-1}$  greater than the range for El Dorado. Salinity is a diagnostic tool which distinguishes between lower salinity Pacific Ocean vs. higher salinity Gulf of California water masses (Figure 2). Unlike the monotonic increase of temperature with depth, the salinity gradients reversed with lower salinity water often found at depth. At ED, there was a consistent seasonal pattern at 40 m with lower salinity water observed summer/fall and higher salinity water in spring. At CP, only two large intrusions of low salinity water at 40 m occurred in October 2004 and April 2005. These conditions are indicated by higher salinity at 40 m (red lines) and occurred at both the ED and CP moorings.